HAL
open science

Piezo1 is required for outflow tract and aortic valve development.

Adèle Faucherre, Hamid Moha Ou Maati, Nathalie Nasr, Amélie Pinard, Alexis Theron, Gaelle Odelin, Jean-Pierre Desvignes, David Salgado, Gwenaëlle Collod-Beroud, Jean-François Avierinos, et al.

To cite this version:

Adèle Faucherre, Hamid Moha Ou Maati, Nathalie Nasr, Amélie Pinard, Alexis Theron, et al.. Piezo1 is required for outflow tract and aortic valve development.. Journal of Molecular and Cellular Cardiology, 2020, 143, pp.51-62. 10.1016/j.yjmcc.2020.03.013 . hal-02863713

HAL Id: hal-02863713

https://hal.science/hal-02863713v1

Submitted on 11 Nov 2020

HAL is a multi-disciplinary open access archive for the deposit and dissemination of scientific research documents, whether they are published or not. The documents may come from teaching and research institutions in France or abroad, or from public or private research centers.

L'archive ouverte pluridisciplinaire **HAL**, est destinée au dépôt et à la diffusion de documents scientifiques de niveau recherche, publiés ou non, émanant des établissements d'enseignement et de recherche français ou étrangers, des laboratoires publics ou privés.

Piezo1 is required for zebrafish outflow tract and aortic valve development.

(Piezo1 and outflow tract/aortic valve development)

*†Adèle Faucherre[1], †Hamid Moha ou Maati[1], Nathalie Nasr[1], Amélie Pinard[2], Alexis Theron[2,3], Gaëlle Odelin[2], Jean-Pierre Desvignes[2], David Salgado[2], Gwenaëlle Collod-Béroud[2], Jean-François Avierinos[2,4],Guillaume Lebon[1], *Stéphane Zaffran[2], *Chris Jopling[1]*

[1] Institut de Génomique Fonctionnelle, Université de Montpellier, CNRS, INSERM LabEx ICST, Montpellier, France
[2]Aix Marseille Univ, INSERM, MMG UMR1251, 13005 Marseille, France.

[3]Service de Chirurgie Cardiaque, AP-HM, Hôpital de la Timone, 13005, Marseille, France.

[4]Service de Cardiologie, AP-HM, Hôpital de la Timone, 13005, Marseille, France.

Corresponding authors-

Chris Jopling, PhD, Email: chris.jopling@igf.cnrs.fr

Stephane Zaffran PhD, Email: stephane.zaffran@univ-amu.fr

† Co-first authors.

*Co-corresponding authors.

Abstract

Aims- During embryogenesis, the onset of circulatory blood flow generates a variety of hemodynamic forces which reciprocally induce changes in cardiovascular development and performance. It has been known for some time that these forces can be detected by as yet unknown mechanosensory systems which in turn promote cardiogenic events such as outflow tract and aortic valve development. PIEZO1 is a mechanosensitive ion channel present in endothelial cells where it serves to detect hemodynamic forces making it an ideal candidate to play a role during cardiac development. We sought to determine whether PIEZO1 is required for outflow tract and aortic valve development.

Methods and results-By analysing heart development in zebrafish we have determined that *piezo1* is expressed in the developing outflow tract where it serves to detect hemodynamic forces. Consequently, disrupting Piezo1 signalling leads to defective outflow tract and aortic valve development and indicates this gene may be involved in the etiology of congenital heart diseases. Based on these findings, we analysed genomic data generated from patients who suffer from left ventricular outflow tract obstructions (LVOTO) and identified 3 probands who each harboured potentially pathogenic variants in *PIEZO1*. Subsequent *in vitro* and *in vivo* assays indicates that these variants behave as dominant negatives leading to an inhibition of normal PIEZO1 mechanosensory activity. Expressing these dominant negative *PIEZO1* variants in zebrafish endothelium leads to defective aortic valve development.

Conclusion- These data indicate that the mechanosensitive ion channel *piezo1* is required for OFT and aortic valve development.

Introduction

In many species, the onset of circulation precedes the role it will play later in life as an oxygen and nutrient delivery system[1]. As the primitive heart initiates circulation, the forces generated by the blood flow are detected by mechanosensory systems present in the endothelium which lines both the heart and vasculature[2]. These extracellular forces are subsequently converted into intracellular signals which can trigger a variety of cellular responses[3]. Many lines of evidence suggest that the hemodynamic forces generated by the circulatory system act as epigenetic cues to drive developmental processes such as cardiogenesis and valvulogenesis forward[4, 5]. Although a number of mechanosensory systems with the potential to sense circulatory hemodynamics have been identified, our knowledge of how the endothelium detects mechanical stimuli is far from complete[2, 6]. PIEZO1 is a mechanosensitive ion channel present in the cell membrane. When the cell membrane is stretched, this opens the channel and allows an influx of cations[7]. Recently, PIEZO1 has been shown to confer mechanosensitivity to endothelial cells allowing them to detect hemodynamic shear stress and subsequently align themselves in the correct orientation during vasculogenesis[8, 9]. Furthermore, deleterious mutations in *PIEZO1* are associated with lymphedema in humans which is caused by defective lymphatic valve development[10].

The outflow tract (OFT) is a transient structure which is extensively remodeled during development and will give rise to a variety of cardiovascular structures including the aortic and pulmonary valves. Although it is well established that hemodynamic blood flow plays a role in OFT development and the formation of the aortic valves[11], the mechanosensors that detect these forces have remained elusive. However, because of its role in sensing shear stress in the vasculature, *PIEZO1* makes a promising candidate for detecting similar forces in the OFT.

Here we report that disrupting Piezo1 signalling in zebrafish leads to defective development of the OFT and aortic valves. Based on these findings we have been able to

identify 3 independent predicted pathogenic *PIEZO1* variants in patients with LVOTO. Furthermore, *in vitro* electrophysiological analysis indicates that all variants are dominant negatives which significantly inhibit wild type PIEZO1 activity and affect aortic valve development when expressed in the zebrafish endothelium.

Methods

Zebrafish strains and husbandry.

Zebrafish were maintained under standardized conditions and experiments were conducted in accordance with local approval (APAFIS#4054-2016021116464098 v5) and the European Communities council directive 2010/63/EU. Embryos were staged as described [12]. The *Tg(fli1a:GFP)y1Tg* was provided by the CMR[B] *Centro de Medicina Regenerativa de Barcelona. The double transgenic line Tg(fli1a:GFP)y1;Tg(cmlc2a:RFP)* was generated in house. All larvae were euthanised by administration of excess anaesthetic (Tricaine).

Aortic valve imaging

One day prior imaging, larvae were incubated in 0.2 μM BODIPY-FL Ceramide (Invitrogen D3521) in Embryo medium + PTU (0.003% 1-phenyl-2-thiourea). Larvae were then anesthetized with Tricaine (0.16g/L) and mounted in low melting agarose. Imaging was performed with a Zeiss LSM710 two-photon microscope coupled to a Ti:sapphire laser (Spectra-Physics, Santa Clara, CA, USA) and a water immersion 25× objective.

Electrophysiology

All electrophysiological experiments were performed after 2-6 days of culture for transfected HEK-293T cells seeded at a density of 20 000 cells/35mm dish and after 2-8 hours of culture

101 of freshly dissociated embryonic zebrafish endothelial cells. Dishes were placed on an inverted
102 microscope (DIAPHOT 300, Nikon). Recordings were performed in inside out or cell attached
103 configuration for the patch clamp technique. PIEZO1 currents were elicited by a negative
104 pressure step from 0 to -80mmHg with -10mmHg step increments at -80mV potential.
105 Stimulation protocols and data acquisition were carried out using a PC (Hewlett Packard) with
106 commercial software and hardware (pClamp 10.4) (supplemental information).
107

108 **Exome sequencing**

109 The exonic sequences were captured with the Agilent Sure Select All Exon v4 kit (Agilent,
110 Santa Clara, CA, USA) and sequencing was performed on an Illumina HiSeq2000 sequencing
111 apparatus (Illumina, San Diego, CA, USA). Raw Exome sequencing data were aligned against
112 the human reference genome hs37decoy5 and duplicated reads were identified using the SNAP
113 alignment tool version 1.0beta23. For detailed information regarding coverage etc, see
114 (Suppl.table.2). GATK 3.4 was used to perform local indel realignment, score base recalibration
115 and variant calling with the Haplotype Caller. Variations were then selected based on quality
116 criteria using the Variant Filtration module from GATK. Variant annotation (ANNOVAR) and
117 prioritization was performed with the VarAFT software (http://varaft.eu). Prioritization of the
118 filtered-in variants was based on expression in aortic valve according to RNA-seq expression
119 data. Patient recruitment was approved by the Comité de Protection des Patients (13.061).
120

121 **Results**

122 **Identifying the zebrafish endothelial *PIEZO1* ortholog**

123 Previous research has identified a zebrafish *PIEZO1* ortholog that does not appear to be
124 expressed in endothelial cells[13]. We have subsequently identified a second *PIEZO1* ortholog,
125 *piezo1b* (Suppl.Fig.S1). At 24 hours post fertilization (hpf), we could detect a weak *piezo1b*

126 signal in the developing heart tube (Suppl.fig.2.A). By 48hpf a strong expression of *piezo1b*
127 appeared in the AV canal and OFT (Suppl.fig.2.B). By 4 days post fertilization (dpf) we were
128 able to observe a strong expression of *piezo1b* in the OFT and vasculature (Fig.1.A,B and
129 suppl.fig.2.C). Furthermore, we were also able to co-localise *piezo1b* with GFP labelled
130 endothelial cells in the OFT and endocardium and were unable to detect any co-localisation
131 with GFP labelled myocardium (Fig.1.C-E and suppl.fig.2.D-I). These results indicate that
132 *piezo1b* is expressed in endothelial cells during zebrafish development, similar to its
133 mammalian counterpart[9].
134 We next sought to determine whether Piezo1b is a functional mechanosensitive ion channel in
135 the developing zebrafish endothelium. To achieve this, we performed electrophysiological
136 analysis of cultured zebrafish sorted endothelial cells subjected to mechanical stimulation
137 (Fig.1.F,G). Furthermore, we found that knockdown of *piezo1b* abolishes mechanically induced
138 currents which was not the case when we targeted *piezo2*[14] its ortholog (Fig.1.F,G). As an
139 additional control, we performed the same electrophysiological analysis on WT endothelial
140 cells treated with the PIEZO channel inhibitory peptide GsMTx4[15] and also observed a
141 reduction in the amplitude of mechanically induced currents (Fig.1.F,G). These data indicate
142 that Piezo1b is a functional mechanosensitive ion channel present in the endothelial cells of
143 developing zebrafish embryos.
144
145 ***Piezo1b* is involved in cardiovascular development**
146 Knockdown of *piezo1b* produced a phenotype characterized by defective cardiogenesis and
147 associated oedema at 3dpf (Fig.2. A-D'). Because Pz1b expression is not restricted to the
148 endocardium but also appears in vascular endothelial cells, we injected Pz1b-MO1 into
149 *Tg(fli1a:GFP)y1Tg* embryos in which all endothelial cells express GFP, clearly delineating the
150 developing vasculature. Overall, vasculogenesis appears largely unaffected and we were unable

151 to detect any noticeable differences in *fli1a* driven GFP expression (Suppl.fig.S3.S-V).
152 However we were able to detect a few abnormally branched blood vessels associated with the
153 intersegmental veins of the trunk in Pz1b *Tg(fli1a:GFP)y1Tg* morphants, a phenotype which
154 did not occur in any of the un-injected *Tg(fli1a:GFP)y1Tg* embryos (Suppl.fig.S3.U,V).
155 Although we ensured the specificity of the observed phenotype to the knockdown of *piezo1b*
156 by employing two different morpholinos targeting the same gene, we also analysed mRNA
157 splicing, morpholino synergy and generated a CRISPR/Cas9 *piezo1b* knockout
158 (Suppl.information and suppl.figs.S3 and S4). We next sought to rescue the *piezo1b* morphant
159 phenotype using mouse *piezo1* mRNA (mPz1) which is not targeted by the *piezo1b* morpholino
160 (Pz1b-MO1). In this manner, we found that co-injection of Pz1b-MO1 with 20pg of mPz1 RNA
161 could rescue the cardiac defects observed in *piezo1b* morphants (Suppl.fig.S3.C-F). Analysis
162 of a number of physiological parameters indicates that *piezo1b* morphants exhibit a decreased
163 cardiac output along with blood regurgitation through the AV canal (Fig.2.E-I and
164 suppl.information and suppl.fig.S5 and movies S1, S2). Taken together these data indicate that
165 loss of *piezo1b* results in defective cardiac development.
166
167 ***Piezo1b* is required for OFT development**
168 Because the OFT is directly adjacent to the ventricle, it is most likely subjected to some of the
169 most extreme hemodynamic forces which in turn could be detected by Piezo1b to subsequently
170 initiate the further development of this structure. To test this premise we analysed the dynamics
171 of the OFT in living zebrafish larvae using live confocal microscopic imagery to focus on a
172 plane which bisected the OFT. At 2dpf (a time point analogous to the images observed in Fig.2.J
173 and K) we were able to observe the OFT stretch and relax during the cardiac cycle. At the end
174 of systole, the OFT achieved a maximum peak inside diameter of 16.87μm (+/-0.24 SEM)
175 (Fig.2.Q and S and movie S3), whereas during diastole the diameter was reduced to 0μm as the

176 OFT relaxed (Fig.2.R and S and movie S3). We also made similar measurements of the dorsal
177 aorta as a comparison and found that its diameter increased by only 0.72µm (+/-0.20 SEM)
178 during systole (Fig.2.S and movie S4). This indicates that indeed hemodynamic forces produce
179 a strong dynamic response in the OFT endothelium which could potentially be detected by
180 mechanosensors such as Piezo1b.
181 To determine whether Piezo1b is required for OFT development we analysed this structure in
182 WT and *piezo1b* morphants. At 48hpf, we could not detect any discernible differences between
183 WT and *piezo1b* morphant embryos (Fig.2.J,K). However, by 72hpf, the WT OFT had
184 developed into a "pear shaped" structure which was noticeably wider at the interface with the
185 myocardium when compared to the *piezo1b* morphant OFT (Fig.2.L-P). Furthermore we were
186 able to rescue this defect by co-injecting mouse *Piezo1* RNA (Suppl.fig.S3.Q,R). Another
187 prominent feature of OFT development in zebrafish is the strong expression of *elastin* in this
188 region. Zebrafish possess two *elastin* paralogs, *elastin A* (*elnA*) and *elastin B* (*elnB*). Previous
189 research indicates that *elnA* is expressed earliest at around 2dpf in the developing jaw cartilage
190 and OFT. *ElnB* can be detected at 3dpf and becomes predominantly and strongly expressed in
191 the OFT [16]. We confirmed these results by performing whole mount *in situ* hybridisation (ISH)
192 using probes specific for either *elnA* or *elnB*. We were unable to detect expression of either
193 gene in the OFT at 2dpf. However by 3dpf there was a pronounced expression of *elnB* in the
194 OFT region while *elnA* was also expressed in this region albeit to a lesser extent (Fig.3.A,B).
195 To determine the cellular source of ElnB we performed immunohistochemistry using an anti-
196 ElnB antibody on *Tg(fli1a:GFP)y1*. Accordingly, we were able to detect ElnB protein being
197 produced around the OFT, however it did not co-localise with the endothelium and appears
198 instead to be produced by a population of cells which ensheathe the OFT endothelium (Fig.3.C-
199 E). To determine whether *elnB* expression is reliant on *pz1b,* we analysed its expression in
200 *piezo1b* morphants. We found that *elnB* expression was severely diminished in the OFT of

201 *piezo1b* morphants when compared to control embryos (Fig.3.F and G.). Furthermore, we found
202 that co-injection of mouse *Piezo1* mRNA was able to significantly restore *elnB* expression in
203 the OFT of *piezo1b* morphants (Fig.3.H and I). How *piezo1b* is regulating *elnB* expression is at
204 present unclear, potentially it could be *via* a intercellular signaling mechanism triggered by
205 *piezo1b* in the endothelium or *via* a intracellular signaling mechanism triggered by *piezo1b* in
206 the cells which ensheathe the OFT.

207

208 ***Piezo1b* is required for aortic valve development**

209 During cardiac development, the aortic valves will form in the OFT, a process reliant on
210 hemodynamic forces. Based on this notion we analysed the developing aortic valves to
211 determine whether *piezo1b* is involved in this process. To achieve this we labelled 7dpf larvae
212 with BODIPY and imaged them using 2 photon microscopy, a technique which has previously
213 been employed to analyse the development of the atrioventricular valves in zebrafish[17]. Our
214 analysis of WT larvae indicates that at this time point two defined leaflets have formed which
215 function effectively to regulate the flow of blood as it is ejected from the ventricle (Fig.4.A and
216 Movie.S5). In comparison, the valves in *piezo1b* morphants are highly dysmorphic and appear
217 to be enlarged and misshapen (Fig.4.B and Movie.S6). A similar aortic valve phenotype is also
218 apparent in decompensated NMDI treated *piezo1b* KO larvae (Suppl.Fig.S6.). To assess this in
219 more detail we performed a quantification of the defective valves by dividing the length of
220 either leaflet by its width (Fig.4.F and suppl.Fig.S6). We observed a significant reduction in the
221 length/width ratio in *piezo1b* morphants compared to un-injected wildtype larvae indicating that
222 the aortic valves have failed to develop normally.

223 Previous research in mammals and humans has determined that *NOTCH1* is required for aortic
224 valve development and mutations in this gene are associated with BAV, a common cause of
225 left ventricular outflow tract obstruction (LVOTO)[18]. In this regard we next analysed the aortic

226 valves in *notch1b* KO zebrafish larvae. Similar to *piezo1b* morphants, the aortic valves in
227 *notch1b* mutants are also highly dysmorphic compared to WT controls (Fig.4.C,F and
228 Movie.S7). The *epidermal growth factor receptor* (EGFR) gene has also been implicated in the
229 etiology of LVOTO[19], furthermore previous research in zebrafish has indicated that chemical
230 inhibition of EGFR using either PKI166 or AG1478 results in defective OFT development[20].
231 Based on this we treated zebrafish embryos with either inhibitor for 7 days and again assessed
232 aortic valve development. As with *piezo1b* morphants and *notch1b* mutants, inhibition of EGFR
233 results in dysmorphic aortic valves (Fig.4.D,E,F). Taken together these data indicate that loss
234 of *piezo1b* results in defective aortic valve development and, furthermore, the resulting
235 phenotype is reminiscent of the valve phenotype caused by disrupting LVOTO associated
236 genes/proteins in zebrafish. Lastly, based on the phenotypic similarities between *piezo1b*
237 morphants and larvae in which either NOTCH or EGFR signalling has been disrupted, we
238 sought to determine whether Piezo1b could in fact be a downstream component of either of
239 these signalling pathways. To meet this end we performed *in situ* hybridisation for *piezo1b* on
240 either *notch1b* mutants or EGFR inhibitor treated larvae. In this manner we were unable to
241 detect any noticeable difference in *piezo1b* expression in either condition and confirmed this
242 finding by qPCR (Suppl.fig.S7). This indicates that Piezo1b is not a downstream component of
243 either the NOTCH or EGFR signalling pathways.
244
245
246 **Identification of pathogenic *PIEZO1* variants.**
247 To identify pathogenic mutations in *PIEZO1* we examined whole exome sequence data
248 generated in-house from 19 patients diagnosed with LVOTO, a spectrum of conditions we
249 believed encompassed the phenotype we observed in zebrafish. In parallel, we also analysed
250 whole exome sequence data from 30 LVOTO patients provided by the National Heart, Lung,

251 and Blood Institute (NHLBI) Bench to Bassinet Program: The Pediatric Cardiac Genetics
252 Consortium (PCGC) dataset (dbGaP accession phs000571.v3.p2.). In this manner, we were able
253 to identify 3 independent nonsynonymous variants in *PIEZO1*: p.Tyr2022His (c.6064T>C;
254 p.Y2022H; located in a transmembrane C-terminal domain (in-house analysis)), p.Lys2502Arg
255 (c.7505A>G; p.K2502R; located in the cytoplasmic C-terminal region of PIEZO1 (in-house
256 analysis)) and p.Ser217Leu (c. 650C>T; p.S217L; located in N-terminal region (PCGC
257 analysis)) (Fig.5.A-C). The heterozygous p.Y2022H and p.K2502R variants were subsequently
258 validated by Sanger sequencing (Fig.5.B,C). Although this was not possible for the p.S217L
259 variant, we were able to determine that one of the parents also harboured this mutation
260 indicating that the proband is heterozygous for this variant. According to gnomAD[21], all 3
261 variants are considered rare, with minor allele frequencies <1% (Table.1). By comparing
262 PIEZO1 orthologs in different species it is apparent that Tyr_{2022}, Lys_{2502} and Ser_{217} are
263 evolutionary conserved amino acids (Fig.5.F). To determine the potential functional
264 consequences these variants have on PIEZO1, they were analysed using the CADD[22], Mutation
265 Taster2[23] and UMD Predictor programs[24] (Table.1). In this manner, all 3 variants are predicted
266 to be pathogenic. Interestingly the diagnostic phenotype which is common to all 3 probands is
267 bicuspid aortic valve disease (BAV).

268

269 **Clinical analysis of patients harboring variants in *PIEZO1.***

270 The BAV phenotype found in the p.Y2022H and p.K2502R probands was diagnosed by
271 echocardiography (Fig.5.G-I). The proband carrying the p.Y2022H (c.6064T>C) variant was
272 diagnosed in childhood with several congenital malformations including a BAV without
273 ascending aorta aneurysm, a left arm agenesis, a bicornate uterus and a urogenital malformation.
274 Physical examination revealed an aortic murmur at the third intercostal space. Transthoracic
275 echocardiography showed a BAV (Fig.5.H and movie S8) with a raphe between the right and

276 the non-coronary leaflets (so called I, R/NC, regarding the Sievers classification) and a mild-
277 to-moderate aortic regurgitation (Effective regurgitant orifice area = 16mm²) due to a prolapse
278 of the anterior leaflet.
279 The proband carrying the p.K2502R (c.7505A>G) variant was incidentally diagnosed at 13
280 years old. Family medical history revealed that his mother had a mitral valve prolapse.
281 However, we have no further information on the mother's genotype. Physical examination
282 revealed a 3/6 holodiastolic murmur. Transthoracic echocardiography showed a BAV (Fig. 5.I,
283 and movie S9) with a raphe between the right and the left coronary leaflets (I, R/L, regarding
284 the Sievers classification) and a moderate aortic regurgitation (Effective regurgitant orifice area
285 = 20mm²) due to a prolapse of the anterior leaflet. There was no dilatation of the ascending
286 aorta. Left ventricular ejection fraction was 70%.
287 The proband (dbGaP Subject ID-711051) harboring the p.S217L (c. 650C>T) variant was
288 diagnosed in adolescence (age 17.3 years old) by echocardiography with a BAV R/NC fusion.
289 Further cardiac analysis revealed no other associated cardiac defects (cardiac situs, systemic
290 vein, hepatic vein, pulmonary vein, right atrium, atrial septum, left atrium, atrioventricular
291 junction, tricuspid valve, mitral valve, right ventricle, left ventricle, pulmonary valve, coronary
292 arteries, pulmonary arteries and aorta are normal). The proband is a caucasian male born in the
293 United States of America, he stands at 162.2cm tall and weighs 117kg, he presented with no
294 other extra cardiac abnormalities. His mother and father are caucasian Americans and were 22
295 and 26 years of age respectively at the birth of the proband. The mother also harbors the same
296 p.S217L variant. Although the mother has no reported history of heart disease, we have no
297 information regarding whether or not she has undergone echocardiography to detect BAV (a
298 limitation of the study recognized by the PCGC). No further information regarding the mother
299 is available. Although it is very interesting to note that all 3 probands have been diagnosed with

300 BAV it will require a much larger cohort and detailed familial data to determine whether or not
301 *PIEZO1* is indeed associated with this condition.

302

303 **Functional analysis of pathogenic *PIEZO1* variants.**

304 To determine whether the identified variants affected PIEZO1 protein function, we performed
305 mechano-electrophysiology analysis of HEK-293T cells transfected with either wildtype (WT)
306 human *PIEZO1* or the p.Y2022H, p.K2502R and p.S217L variants. In this manner we were
307 able to detect changes in current from HEK cells transfected with wildtype human *PIEZO1*
308 (Fig.5.A,E). Conversely, cells which had been transfected with either p.Y2022H, p.K2502R or
309 p.S217L *PIEZO1* variants showed significantly reduced mechano-stimulated currents (Fig.5.B-
310 E). One explanation for the reduction in *PIEZO1* activity associated with these variants is that
311 the mutations result in a reduction of cell surface expression. To assess this possibility we
312 performed immunohistochemistry (IHC) on HEK-293T cells transfected with either wildtype
313 human *PIEZO1* the p.Y2022H, p.K2502R or p.S217L *PIEZO1* variants. Confocal images of
314 transfected cells indicates that none of the variants appear to significantly affect the localization
315 of PIEZO1 to the cell surface when compared to wildtype PIEZO1 (Fig.5.F). To confirm this
316 observation we measured the fluorescent intensity across the cell membrane. In this manner,
317 wildtype PIEZO1 and all of the variants show a clear peak of intensity at the cell surface which
318 drops sharply on the extracellular and intracellular sides when compared to GFP, which is
319 expressed throughout the cell (Fig.5.G). This shows that aberrant trafficking of PIEZO1 to the
320 cell surface is not the reason for the observed reduction in activity. These data indicate that the
321 variants p.Y2022H, p.K2502R and p.S217L have deleterious effects on PIEZO1 protein
322 function.

323

324 **p.Y2022H, p.K2502R and p.S217L *PIEZO1* variants are dominant negative isoforms.**

325 Because all 3 probands are heterozygous for their respective variants, we next sought to
326 ascertain whether these variants were dominant negatives. When wildtype human *PIEZO1* was
327 co-transfected with either p.Y2022H, p.K2502R or p.S217L *PIEZO1* variants, there was a
328 significant decrease in current amplitude compared to the control (Fig.6.A-E). Taken together
329 these data indicate that the p.Y2022H, p.K2502R and p.S217L *PIEZO1* variants act as dominant
330 negatives.

331 Next we sought to determine whether expression of the dominant negative human
332 *PIEZO1* variants in the zebrafish endothelium could also affect aortic valve development. To
333 achieve this we generated a transgenic construct using a previously characterised endothelial
334 specific *fliEP* promoter[25] to drive expression of either WT *PIEZO1* or the variants specifically
335 in endothelial cells *in vivo* (Suppl.fig.S8.A-G). In this manner we were able to determine that
336 expressing any of the dominant negative variants (p.Y2022H, p.K2502R or p.S217L) also had
337 a significant impact on aortic valve development when compared to WT *PIEZO1* endothelial
338 expression. To assess this in more detail we performed a quantification of the defective valves
339 by dividing the length of either leaflet by its width (Fig.7.A,B). In this manner we found that
340 all the variants significantly reduced the overall length/width ratio in both leaflets when
341 compared to the WT *PIEZO1* expressing larvae. This indicates that expression of either
342 Y2022H, p.K2502R or p.S217L *PIEZO1* disrupts aortic valve development in zebrafish.

343

344 **Discussion**

345 Here we have shown that the mechanosensitive ion channel Piezo1b is required for OFT/aortic
346 valve development in zebrafish. In particular knockdown of *piezo1b* mRNA leads to a
347 constricted OFT and dysmorphic aortic valves. We have also identified 3 novel pathogenic
348 *PIEZO1* variants in patients who suffer from LVOTO. All 3 variants are dominant negative

349 isoforms which when expressed in the developing zebrafish endothelium disrupt aortic valve
350 development, confirming our results achieved by *piezo1b* knockdown. We believe that this is
351 the first description of dominant negative PIEZO1 isoforms and future research will be required
352 to determine whether these variants are indeed associated with LVOTO. However, our data
353 does highlight a role for Piezo1b in the developing zebrafish OFT and aortic valves where it
354 serves to detect hemodynamic forces associated with the cardiac cycle and subseqeuntly drive
355 development forward, which would fit with a role for this gene in the etiology of LVOTO.
356 Although our data indicate that *piezo1b* is required in the endothelium during aortic valve
357 development it should also be stressed that other cell types involved in this process, such as
358 smooth muscle cells (SMC), may also require *piezo1b*. Indeed a recent study by Duchemin *et*
359 *al*, which corroborates many of our own findings, indicates that *piezo1* expressing SMC play a
360 significant role in aortic valve development[26].

361 Despite the differences in cardiac physiology, early OFT development is highly
362 conserved between mammals and zebrafish, in particular this region will give rise to the aortic
363 valves. Indeed, elegant studies in avian models have indicated that disrupting hemodynamic
364 forces, either by increasing or decreasing flow/pressure, significantly disrupts a variety of
365 cardiac developmental processes including OFT and aortic valve development[27]. Recently, it
366 has been established that in developing zebrafish larvae the coordinated actions of the
367 mechanosensitive ion channels TRPV4 and TRPP2 are required to promote *klf2a* expression in
368 the atrioventricular canal and subsequently drive valve morphogenesis in this region[28]. Our data
369 indicates that Piezo1 plays a similar role in the developing OFT region. Another gene which
370 has been implicated in aortic valve development is EGFR due to its association with BAV in
371 humans[29]. Likewise, *Egfr* KO mice (also known as Wave mice) develop abnormal, functionally
372 defective aortic valves resulting in regurgitation of blood through this region[30]. Previously it
373 has been shown that treatment of zebrafish larvae with the EGFR inhibitors PKI166 and

374 AG1478 results in defective OFT development[20]. In agreement with these findings our own
375 data indicates that Egfr is required for aortic valve development in zebrafish and when this
376 process is disrupted this results in a defective valve phenotype very similar to that observed in
377 *piezo1b* morphants. *NOTCH1* is one of the few genes directly linked to BAV in humans[18]. Our
378 own data indicates that the zebrafish *NOTCH1* ortholog *notch1b* also regulates aortic valve
379 development. Indeed, zebrafish *notch1b* mutants display dysmorphic valves. Importantly, we
380 also observed a very similar aortic valve phenotype in *piezo1b* morphant larvae indicating that
381 this gene is also required for aortic valve development. Although our data indicates that Piezo1b
382 is not a downstream component of either NOTCH or EGFR signaling pathways future
383 investigations will be aimed at trying to ascertain whether any synergy exists between these
384 pathways during aortic valve development. Lastly, all 3 probands have been diagnosed with
385 bicuspid aortic valve (BAV), however it will require a much larger cohort and detailed familial
386 data to determine whether or not *PIEZO1* is indeed associated with this condition.
387

388 **Funding**

389 This work was supported by INSERM and CNRS. Work in the C.J lab is supported by a grant
390 from the Fondation Leducq. Work in the C.J lab is supported by a grant from Fondation pour
391 la Recherche sur le Cerveau "Espoir en tête 2017". C.J was supported by an INSERM ATIP-
392 AVENIR grant and a Marie Curie CIG (PCIG12-GA-2012-332772). H.M.M is supported by a
393 grant from the Association Française contre les Myopathies (AFM-Telethon). A.F was
394 supported by a Fondation Lefoulon-Delalande postdoctoral fellowship with previous support
395 provided by a Fondation pour la Recherche Médicale (FRM) postdoctoral fellowship. N.N is
396 supported by the LabexICST PhD program. A.F, H.M.M, N.N and C.J are members of the
397 Laboratory of Excellence « Ion Channel Science and Therapeutics » supported by a grant from
398 the ANR. A.P. received a PhD fellowship from the Association Française du Syndrome de

Marfan et Apparentés (AFSMa). Work in the G.L lab is supported by a grant from the ANR (ANR 17 CE18 0001 06 AT2R TRAAK).Work in S.Z lab is supported by the INSERM and the Association Française contre les Myopathies (AFM-Telethon). IPAM acknowledges the France-BioImaging infrastructure supported by the French National Research Agency (ANR-10-INBS-04, «Investments for the future»), the Fondation pour la Recherche sur le Cerveau "Espoir en tête 2015", and Fondation Leducq.

Acknowledgements

We would like to acknowledge Dr Matteo Mangoni and Dr Joel Nargeot for their input and support. We would like to thank Prof Ardem Patapoutian for the kind gift of h*PIEZO1*-pIRES2-GFP. We would like to thank Dr Emmanuel Bourinet for the kind gift of m*Piezo1*. We would like to thank Dr Yaniv Hintis (Kings College London, UK) and Prof Fred Keeley and Dr Megan Miao (Hospital for Sick Children, Toronto, CA) for kindly donating the ElnB antibody. We would also like to acknowledge the Montpellier MGX Genomix platform for their input and support. Part of this data was generated by the Pediatric Cardiac Genomics Consortium (PCGC), under the auspices of the National Heart, Lung, and Blood Institute's Bench to Bassinet Program <http://www.benchtobassinet.org/>. The Pediatric Cardiac Genomics Consortium (PCGC) program is funded by the National Heart, Lung, and Blood Institute, National Institutes of Health, U.S. Department of Health and Human Services through grants U01HL098123, U01HL098147, U01HL098153, U01HL098162, U01HL098163, and U01HL098188. This manuscript was not prepared in collaboration with investigators of the PCGC, has not been reviewed and/or approved by the PCGC, and does not necessarily reflect the opinions of the PCGC investigators or the NHLBI. We thank Anthony Pinot from the *in vivo* imaging platform IPAM-Biocampus Montpellier.

Conflicts of Interests

None declared

References

1. Granados-Riveron JT, Brook JD. The impact of mechanical forces in heart morphogenesis. *Circ Cardiovasc Genet* 2012;**5**:132-142.
2. Freund JB, Goetz JG, Hill KL, Vermot J. Fluid flows and forces in development: functions, features and biophysical principles. *Development* 2012;**139**:1229-1245.
3. Lansman JB, Hallam TJ, Rink TJ. Single stretch-activated ion channels in vascular endothelial cells as mechanotransducers? *Nature* 1987;**325**:811-813.
4. Goetz JG, Steed E, Ferreira RR, Roth S, Ramspacher C, Boselli F, Charvin G, Liebling M, Wyart C, Schwab Y, Vermot J. Endothelial cilia mediate low flow sensing during zebrafish vascular development. *Cell Rep* 2014;**6**:799-808.
5. Hove JR, Koster RW, Forouhar AS, Acevedo-Bolton G, Fraser SE, Gharib M. Intracardiac fluid forces are an essential epigenetic factor for embryonic cardiogenesis. *Nature* 2003;**421**:172-177.
6. Busse R, Fleming I. Vascular endothelium and blood flow. *Handb Exp Pharmacol* 2006:43-78.
7. Coste B, Xiao B, Santos JS, Syeda R, Grandl J, Spencer KS, Kim SE, Schmidt M, Mathur J, Dubin AE, Montal M, Patapoutian A. Piezo proteins are pore-forming subunits of mechanically activated channels. *Nature* 2012;**483**:176-181.
8. Li J, Hou B, Tumova S, Muraki K, Bruns A, Ludlow MJ, Sedo A, Hyman AJ, McKeown L, Young RS, Yuldasheva NY, Majeed Y, Wilson LA, Rode B, Bailey MA, Kim HR, Fu Z, Carter DA, Bilton J, Imrie H, Ajuh P, Dear TN, Cubbon RM, Kearney MT, Prasad RK, Evans PC, Ainscough JF, Beech DJ. Piezo1 integration of vascular architecture with physiological force. *Nature* 2014.
9. Ranade SS, Qiu Z, Woo SH, Hur SS, Murthy SE, Cahalan SM, Xu J, Mathur J, Bandell M, Coste B, Li YS, Chien S, Patapoutian A. Piezo1, a mechanically activated ion channel, is required for vascular development in mice. *Proc Natl Acad Sci U S A* 2014;**111**:10347-10352.
10. Nonomura K, Lukacs V, Sweet DT, Goddard LM, Kanie A, Whitwam T, Ranade SS, Fujimori T, Kahn ML, Patapoutian A. Mechanically activated ion channel PIEZO1 is required for lymphatic valve formation. *Proc Natl Acad Sci U S A* 2018;**115**:12817-12822.
11. Menon V, Eberth JF, Goodwin RL, Potts JD. Altered Hemodynamics in the Embryonic Heart Affects Outflow Valve Development. *Journal of cardiovascular development and disease* 2015;**2**:108-124.
12. Kimmel CB, Ballard WW, Kimmel SR, Ullmann B, Schilling TF. Stages of embryonic development of the zebrafish. *Developmental dynamics : an official publication of the American Association of Anatomists* 1995;**203**:253-310.
13. Faucherre A, Kissa K, Nargeot J, Mangoni M, Jopling C. Piezo1 plays a role in erythrocyte volume homeostasis. *Haematologica* 2013.
14. Faucherre A, Nargeot J, Mangoni ME, Jopling C. piezo2b regulates vertebrate light touch response. *J Neurosci* 2013;**33**:17089-17094.
15. Bae C, Sachs F, Gottlieb PA. The mechanosensitive ion channel Piezo1 is inhibited by the peptide GsMTx4. *Biochemistry* 2011;**50**:6295-6300.
16. Miao M, Bruce AE, Bhanji T, Davis EC, Keeley FW. Differential expression of two tropoelastin genes in zebrafish. *Matrix biology : journal of the International Society for Matrix Biology* 2007;**26**:115-124.
17. Vermot J, Forouhar AS, Liebling M, Wu D, Plummer D, Gharib M, Fraser SE. Reversing blood flows act through klf2a to ensure normal valvulogenesis in the developing heart. *PLoS Biol* 2009;**7**:e1000246.

471 18. Garg V, Muth AN, Ransom JF, Schluterman MK, Barnes R, King IN, Grossfeld PD, Srivastava D.
472 Mutations in NOTCH1 cause aortic valve disease. *Nature* 2005;**437**:270-274.
473 19. Giusti B, Sticchi E, De Cario R, Magi A, Nistri S, Pepe G. Genetic Bases of Bicuspid Aortic Valve:
474 The Contribution of Traditional and High-Throughput Sequencing Approaches on Research and
475 Diagnosis. *Frontiers in physiology* 2017;**8**:612.
476 20. Goishi K, Lee P, Davidson AJ, Nishi E, Zon LI, Klagsbrun M. Inhibition of zebrafish epidermal
477 growth factor receptor activity results in cardiovascular defects. *Mechanisms of development*
478 2003;**120**:811-822.
479 21. Lek M, Karczewski KJ, Minikel EV, Samocha KE, Banks E, Fennell T, O'Donnell-Luria AH, Ware
480 JS, Hill AJ, Cummings BB, Tukiainen T, Birnbaum DP, Kosmicki JA, Duncan LE, Estrada K, Zhao F,
481 Zou J, Pierce-Hoffman E, Berghout J, Cooper DN, Deflaux N, DePristo M, Do R, Flannick J,
482 Fromer M, Gauthier L, Goldstein J, Gupta N, Howrigan D, Kiezun A, Kurki MI, Moonshine AL,
483 Natarajan P, Orozco L, Peloso GM, Poplin R, Rivas MA, Ruano-Rubio V, Rose SA, Ruderfer DM,
484 Shakir K, Stenson PD, Stevens C, Thomas BP, Tiao G, Tusie-Luna MT, Weisburd B, Won HH, Yu
485 D, Altshuler DM, Ardissino D, Boehnke M, Danesh J, Donnelly S, Elosua R, Florez JC, Gabriel SB,
486 Getz G, Glatt SJ, Hultman CM, Kathiresan S, Laakso M, McCarroll S, McCarthy MI, McGovern D,
487 McPherson R, Neale BM, Palotie A, Purcell SM, Saleheen D, Scharf JM, Sklar P, Sullivan PF,
488 Tuomilehto J, Tsuang MT, Watkins HC, Wilson JG, Daly MJ, MacArthur DG, Exome Aggregation
489 C. Analysis of protein-coding genetic variation in 60,706 humans. *Nature* 2016;**536**:285-291.
490 22. Kircher M, Witten DM, Jain P, O'Roak BJ, Cooper GM, Shendure J. A general framework for
491 estimating the relative pathogenicity of human genetic variants. *Nature genetics* 2014;**46**:310-
492 315.
493 23. Schwarz JM, Cooper DN, Schuelke M, Seelow D. MutationTaster2: mutation prediction for the
494 deep-sequencing age. *Nature methods* 2014;**11**:361-362.
495 24. Salgado D, Desvignes JP, Rai G, Blanchard A, Miltgen M, Pinard A, Levy N, Collod-Beroud G,
496 Beroud C. UMD-Predictor: A High-Throughput Sequencing Compliant System for Pathogenicity
497 Prediction of any Human cDNA Substitution. *Human mutation* 2016;**37**:439-446.
498 25. Villefranc JA, Amigo J, Lawson ND. Gateway compatible vectors for analysis of gene function
499 in the zebrafish. *Developmental dynamics : an official publication of the American Association*
500 *of Anatomists* 2007;**236**:3077-3087.
501 26. Duchemin AL, Vignes H, Vermot J. Mechanically activated piezo channels modulate outflow
502 tract valve development through the Yap1 and Klf2-Notch signaling axis. *eLife* 2019;**8**.
503 27. Poelmann RE, Gittenberger-de Groot AC. Hemodynamics in Cardiac Development. *Journal of*
504 *cardiovascular development and disease* 2018;**5**.
505 28. Heckel E, Boselli F, Roth S, Krudewig A, Belting HG, Charvin G, Vermot J. Oscillatory Flow
506 Modulates Mechanosensitive klf2a Expression through trpv4 and trpp2 during Heart Valve
507 Development. *Current biology : CB* 2015;**25**:1354-1361.
508 29. Dargis N, Lamontagne M, Gaudreault N, Sbarra L, Henry C, Pibarot P, Mathieu P, Bosse Y.
509 Identification of Gender-Specific Genetic Variants in Patients With Bicuspid Aortic Valve. *The*
510 *American journal of cardiology* 2016;**117**:420-426.
511 30. Hajj GP, Chu Y, Lund DD, Magida JA, Funk ND, Brooks RM, Baumbach GL, Zimmerman KA, Davis
512 MK, El Accaoui RN, Hameed T, Doshi H, Chen B, Leinwand LA, Song LS, Heistad DD, Weiss RM.
513 Spontaneous Aortic Regurgitation and Valvular Cardiomyopathy in Mice. *Arterioscler Thromb*
514 *Vasc Biol* 2015;**35**:1653-1662.
515 31. Zhao Q, Zhou H, Chi S, Wang Y, Wang J, Geng J, Wu K, Liu W, Zhang T, Dong MQ, Wang J, Li X,
516 Xiao B. Structure and mechanogating mechanism of the Piezo1 channel. *Nature* 2018;**554**:487-
517 492.

518 **Figure legends**

519 **Figure.1. Identifying the zebrafish endothelial *PIEZO1* ortholog.**

520 (**A,B**) ISH using an antisense *piezo1b* probe. *piezo1b* expression can be detected in the OFT of
521 zebrafish larvae (yellow arrowhead) at 4dpf. (**C-E**) Double fluorescent ISH using antisense
522 GFP (**C**) and antisense *piezo1b* (**D**) probes, merged image (**E**) indicates endothelial GFP and
523 piezo1b co-localise in the OFT endothelium at 4dpf in *Tg(fli1a:GFP)y1* embryos. (**F,G**)
524 Electrophysiological recordings of mechanosensitive currents from embryonic endothelial
525 cells. Currents were recorded via patch clamp using and inside out configuration by application
526 of negative pressures from 0 to -80mmHg with -10mmHg step increments at -80mV potential.
527 (**F**) Typical current traces recorded from cells isolated from control, piezo1b MO1, Pz2 MO
528 injected embryos and cell treated with GsMTx4 *via* the patch clamp pipette. The pressure
529 stimulation protocol is shown in inset. (**G**) Corresponding pressure/current curves showing the
530 activation of the current from control, Pz1b-MO1, Pz2-MO cells and GsMTx4 treated cells (*
531 p<0,05, ** p<0.01, student's t-test). The red rectangle shows the value of the current amplitude
532 for the three test conditions at -50 mmHg step stimulation. Scale bars: (**A,B**) 100μm (**E**) 10μm.
533

534 **Figure.2. *Piezo1b* is involved in cardiovascular development.**

535 (**A**) Un-injected 72hpf zebrafish embryo, (**A'**) the same embryo at higher magnification. (**C**) A
536 72hpf *piezo1b* morphant displaying pericardial oedema and defective cardiac looping (black
537 arrowhead), (**C'**) the same embryo at higher magnification. (n=48/50). (**B,B',D,D'**) ISH using
538 an antisense *cmlc2a* probe on (**B**) 72hpf un-injected zebrafish embryos, (**B'**) the same embryo
539 at higher magnification, the yellow dashed line above the ventricle (v) and atrium (a) is an
540 indicator for the degree of cardiac looping. (**D**) 72hpf *piezo1b* morphant embryo, (**D'**) the same
541 embryo at higher magnification, note the yellow dashed line is no longer horizontal indicating
542 a defect in cardiac looping (n=48/50). (**E**) Graph depicting the average heart rate in beats per
543 minute (BPM) of WT (n=8) and Pz1b morphants (n=8). (**F**) Graph depicting the average blood
544 flow rate in nano litres per second (nL/sec) of WT (n=8) and Pz1b morphants (n=8). (**G**) Graph

545 depicting the average minimum/maximum blood flow rate in nano litres per second (nL/sec) of
546 WT (n=8) and Pz1b morphants (n=8). (**H**) Graph depicting the average stroke volume in nano
547 litres per heart beat (nL/beat) of WT (n=8) and *piezo1b* morphants (n=8). (**I**) Graph depicting
548 the average ventricular contractile distance in micro metres (μM) of WT (n=5) and Pz1b
549 morphants (n=5). (**J-M**) Maximal projections of 48hpf (**J,K**) and 72hpf (**L-M**)
550 *Tg(fli1a:GFP)y1;Tg(cmlc2:RFP)* OFT from WT (**J,L**) and *piezo1b* morphants (**K,M**).Yellow
551 dashed lines delineate the OFT position at 48hpf (**J,K**). (**N,O**) Maximal projections of a 72hpf
552 *Tg(fli1a:GFP)y1* OFT from WT (**N**) and *piezo1b* morphants (**O**). The white line indicates the
553 width of the OFT immediately adjacent to the myocardium. (**P**) Graph showing the average size
554 of the OFT of WT and *piezo1b* morphants(n wt=7, n Pz1bMO1=11). (**Q**) A still image taken
555 from a resonance laser z-stack movie of a live 48hpf *Tg(fli1a:GFP)y1* zebrafish larvae's OFT
556 at the end of systole, the yellow dashed lines delineate the edges of the OFT endothelial vascular
557 walls. The white double headed arrow indicates the OFT inside diameter during systole. (**R**) A
558 still image taken from a resonance laser z-stack movie of a live 48hpf *Tg(fli1a:GFP)y1*
559 zebrafish larvae's OFT during diastole, the yellow dashed lines delineate the edges of the OFT
560 endothelial vascular walls which are in contact with one another. (**S**) Graph showing the
561 difference between OFT and aorta inside diameters between diastole and systole (n=4; 3
562 contractions for each). All graphs (* p<0,05, ** p<0.01, student's t-test),Scale bars (**A-B'**)
563 100μm (**J-O** and **Q,R**) 10μm.
564

565 **Figure.3. *Elastin* expression in the OFT of zebrafish is dependent on *Piezo1b*.**

566 (**A,B**) *In situ* hybridization against *eln*A (**A**) and *elnB* (**B**) on 3 dpf embryos. (**C-E**) Single z-
567 stack confocal images of the OFT following an immunostaining using an anti-ElnB antibody
568 (**C**, red) on 3 dpf *Tg(fli1a:GFP)y1* embryos (**D**, green). The merged image (**E**) indicates that
569 the cells producing ElnB are not endothelial which are producing GFP. (**F,G**)) *In situ*

570 hybridization against *elnB* in 3 dpf WT (**F**) and *piezo1b* (**G**) morphants. (**H**) *In situ* hybridization
571 using an antisense *elnB* probe on *piezo1b* morphant embryos co-injected with mouse *Piezo1*
572 mRNA. Embryos were sorted according to the intensity of *elnB* expression. (**I**) Percentage of
573 embryos showing the *elnB* expression levels depicted in (**M**) in WT, Pz1bMO1 injected or
574 Pz1bMO1 + m*Piezo1* RNA injected embryos.
575
576
577 **Figure.4. *Piezo1b* is required for aortic valve development.**
578 2 photon images of aortic valves in 7dpf zebrafish larvae labelled with BODIPY. **(A)**
579 Representative image of the aortic valves in a WT larvae, valves are outlined with a dashed
580 white line (n=8). **(B)** A *piezo1b* morphant (n=6). **(C)** A *notch1b* mutant (n=11). **(D)** A AG1478
581 treated larvae (n=6). **(E)** A PKI166 treated larvae (n=6). Graph depicting the length to width
582 ratio for the left and right valve leaflets measured in 7dpf WT larvae, Pz1b morphants, *notch1b*
583 KO larvae or larvae treated with either AG1478 or PKI166. Error bars indicate SD, ANOVA
584 and Dunnet's multiple comparisons test P<0.01(all samples), student's unpaired homoscedastic
585 two tailed t-test **P<0.01. Scale bars-20μm.
586
587 **Figure.5. Identification of pathogenic variants in *PIEZO1*.**
588 (**A**) Schematic representation of human PIEZO1 protein, the position of each variant is
589 indicated by a red dot (adapted from *Zhao et al*[31]). (**B,C**) Cartoon representation of the mouse
590 mechanosensitive Piezo1 channel 3D Model (PDB 5Z10). The corresponding residues K2502
591 (Magenta) and Y2022 (Green) identified in this study as subject to genetic variability are
592 represented as spheres. (**D,E**) Sequence chromatographs showing heterozygous variants
593 c.6064T>C (p.Y2022H; B) and c.7505A>G (p.K2502R; C) in genomic DNA taken from the
594 affected LVOTO patients. (**F**) Protein alignments for all 3 variants. Note the strong evolutionary

595 conservation for Tyr2022, Lys2502 and Ser217 residues. (**G-I**) Representative echocardiogram
596 of the aortic valve from an unaffected individual (**G**) and the BAV patients carrying out the
597 c.6064T>C; p.Y2022H variant (**H**) and c.7505A>G; p.K2502R variant (**I**). Note the 3 valve
598 leaflets in the unaffected individual (**G**) compared to the 2 leaflets in the BAV patients (**H** and
599 **I**).
600
601 **Figure.6. Functional analysis of pathogenic *PIEZO1* variants.**
602 Electrophysiological recordings of mechanosensitive currents from all 3 *PIEZO1* variants.
603 Typical current traces recorded from HEK cells transfected with either wildtype (WT) human
604 *PIEZO1* (hPz1) (**A**), human *PIEZO1* c.6064T>C (p.Y2022H) variant (**B**), human *PIEZO1*
605 c.7075A>G (p.K2502R) (**C**) variant or human *PIEZO1* c.650C>T (p.S217L) variant (**D**).
606 Currents were recorded *via* patch clamp using a cell attached configuration by application of
607 negative pressures from 0 to -80mmHg with -10mmHg step increments at -80mV potential. (**E**)
608 Corresponding pressure/current curves showing the activation of the current from wildtype
609 hPz1, p.Y2022H, p.K2502R and p.S217L (* p<0,05, ** p<0.01, *** p<0.001 student's t-test).
610 (**F**) Immunohistochemistry using an anti PIEZO1 antibody on HEK 293T cells transfected with
611 either empty vector (pIRES2-GFP), wildtype human *PIEZO1* (wt-hPz1), human *PIEZO1*
612 c.6064T>C (p.Y2022H) variant (Y2022H-hPz1), human *PIEZO1* c.7075A>G (p.K2502R)
613 variant (K2502R-hPz1) or human *PIEZO1* c.650C>T (p.S217L) variant (S217L-hPz1). **(G)**
614 Cell surface immunofluorescent analysis. Fluorescent intensity was measured in ImageJ by
615 drawing a line through the cell membrane (yellow bar). Graphs plotting the fluorescent intensity
616 at the cell surface for WT and variant *PIEZO1*. In all cases there is a clear peak of RFP
617 fluorescent intensity which tapers off on either side of the cell membrane. The control GFP
618 signal is continuous. Scale bars (F) 10μm.
619

620 **Figure.7. The *PIEZO1* variants are dominant negatives**

621 Electrophysiological recordings of mechanosensitive currents from co-transfection of 3
622 *PIEZO1* variants with wildtype human *PIEZO1*. Typical current traces recorded from HEK
623 cells co-transfected with either wildtype human *PIEZO1* (hPz1) and empty pIRES2-GFP (**A**),
624 wildtype human *PIEZO1* (hPz1) and human *PIEZO1* c.6064T>C (p.Y2022H) variant (**B**),
625 wildtype human *PIEZO1* (hPz1) and human *PIEZO1* c.7075A>G (p.K2502R) variant (**C**) or
626 wildtype human *PIEZO1* (hPz1) and human *PIEZO1* c.650C>T (p.S217L) (**D**). Currents were
627 recorded *via* patch clamp using a cell attached configuration by application of negative
628 pressures from 0 to -80mmHg with -10mmHg step increments at -80mV potential. (**E**)
629 Corresponding pressure/current curves showing the activation of the current from wildtype
630 hPz1/empty pIRES2-GFP, wildtype hPz1/p.Y2022H, wildtype hPz1/p.K2502R and wildtype
631 hPz1/p.S217L (* p<0,05, ** p<0.01, *** p<0.001 student's t-test).

632

633 **Figure.8. Expression of *PIEZO1* variants *in vivo* disrupts aortic valve development**

634 **(A)** Representative images of aortic valve leaflet quantification in a 7dpf larvae expressing
635 either WT human *PIEZO1* (hPZ1-wt) or the Y2022H variant of human *PIEZO1* (hPZ1-
636 Y2022H), ratios were calculated by measuring the length of the leaflet from the lower edge to
637 the tip, the width was measured at a point halfway along the length (yellow lines). **(B)** Graph
638 depicting the length to width ratio for the left and right valve leaflets measured in 7dpf larvae
639 expressing either WT (n=8), K2502R (n=11), Y2022H(n=10) or S217L (n=10) human *PIEZO1*.
640 Error bars indicate SEM, ANOVA and Dunnet's multiple comparisons test P<0.01(all
641 samples), student's unpaired homoscedastic two tailed t-test **P<0.01. Scale bars-20μm.

642

Supplemental information

Morpholinos

The sequences of the injected MOs are the following:

Pz1b MO1: 5′-TCTGTTGCTGGATTCTGTGAATCAT-3’-5ng

Pz1b MO2: 5′-ACCCATGATGCTGCAACACACACAC-3’-4ng

tnnt2 MO : 5′-CATGTTTGCTCTGATCTGACACGCA3’ -3ng

The amount of morpholino used in all experiments is given in nanograms (ng), excluding the suboptimal experiments where the amounts are indicated in the figure (suppl.fig.S3.K-P).

DNA microinjection

The fli1ep:h*PIEZO1* constructs were generated using the Tol2 kit[1]. 478 p5Efli1ep was a gift from Nathan Lawson (Addgene plasmid # 31160 ; http://n2t.net/addgene:31160 ; RRID:Addgene_31160). Wildtype variant h*PIEZO1* were subcloned from pIRES2-GFP into pME-MCS by restriction digestion and ligation. 5' capped sense RNAs were synthesized using a construct encoding the transposase and the mMessage mMachine kit (Ambion). 20 pg of the Fli1ep:hPziezo1 DNA construct and 20 pg of the transposase sRNA were simultaneously injected into embryos at the one cell stage.

Morpholino and CRISPR/Cas9 control experiments

The Pz1b MO1 and MO2 were designed to block the post-transcriptional splicing of the Pz1b. As with Pz1b MO1 (Suppl.fig.S3.A,B), we also confirmed that splicing had been disrupted by performing RT-PCR on Pz1b MO2 morphants (Suppl.fig.S3.I,J). To further ensure that the observed phenotype is due to specific knockdown of Pz1b, we co-injected suboptimal concentrations of both Pz1b MO1 and Pz1b MO2. Subsequent *in situ* hybridization with a *cmlc2a* probe reveals that injection of either morpholino at suboptimal concentrations alone does not affect heart development (Suppl.fig.S3.K-N). However, co-injection of both morpholinos at these concentrations results in the same defective cardiac looping phenotype

26 observed at optimal concentrations of either morpholino (Suppl.fig.S3.O,P). Lastly, we also
27 endeavoured to knockout (KO) Pz1b by employing a CRISPR/Cas9 strategy. To achieve this,
28 we designed a gRNA which targeted exon 11 of Pz1b. In this manner we were able to generate
29 a mutant zebrafish line harbouring a 13bp substitution at position 1435 to 1437 in Pz1b resulting
30 in a frameshift and premature stop codon after 609 amino acids. This line was designated
31 *piezo1b*^{mmr5}. Unfortunately, homozygous *piezo1b*$^{mmr5/\ mmr5}$ embryos did not display any
32 discernible phenotype. A recent report has indicated that KO of the other *piezo1* zebrafish
33 paralogue *piezo1a* also does not produce any discernible phenotype [2]. Although it is possible
34 that zebrafish do not require *piezo1* at all for development, based on the drastic consequences
35 observed in mammals and humans when *piezo1* is KO or mutated, this seems unlikely [3-5].
36 We reasoned that the most likely explanation for the lack of phenotype was due to
37 compensation, as has been reported in other zebrafish KO lines where the expected phenotype
38 was not observed[6]. To assess this possibility we followed the recently developed morpholino
39 guidelines[7] and injected the Pz1b morpholino into embryos from an incross of the
40 *piezo1b*$^{mmr5/mmr5}$ line. If compensation has occurred, we should expect that the Pz1b morpholino
41 would have little effect in homozygous *piezo1b*$^{mmr5/\ mmr5}$ embryos. Indeed, we were able to
42 observe an obvious oedema and defective cardiac looping in wildtype *piezo1b* morphant
43 embryos (the embryos were produced by incrossing a *piezo1b* $^{+/+}$ line which was established in
44 parallel to the KO line to maintain the same genetic background), however this defect was
45 absent in *piezo1b*$^{mmr5/mmr5}$ morphants (Suppl.fig.S4.A-C). This indicates that in *piezo1b*$^{mmr5/\ mmr5}$
46 zebrafish embryos, *piezo1b* is compensated and thus the Pz1b morpholino has little effect. This
47 result also confirms that the phenotype we observe in *piezo1b* morphants is specific to
48 knockdown of Pz1b and is not due to off target effects. To determine whether *piezo1a* could be
49 compensating for the loss of *piezo1b* we performed qPCR for *piezo1a* on *piezo1b*$^{mmr5/\ mmr5}$

50 mutants. However we could not detect any significant upregulation in the expression of *piezo1a*
51 indicating that this gene does not compensate for loss of *piezo1b* (Suppl.Fig.S4.D.).

52 More recently El-Brolosy *et al* have shown that the compensatory mechanism is triggered by
53 the degradation of the mutant mRNA transcript[8]. Indeed, inhibition of nonsense mediated
54 decay with NMDI effectively blocks the compensatory effects observed in mutant zebrafish.
55 We adopted a similar strategy and treated homozygous *piezo1b*$^{mmr5/mmr5}$ embryos with NMDI.
56 In comparison to their wildtype siblings, NMDI treated homozygous *piezo1b*$^{mmr5/mmr5}$ embryos
57 developed a similar cardiac phenotype to that observed in *piezo1b* morphants (Suppl.Fig.6.A.).
58 Furthermore, these larvae also displayed defective aortic valves which were similar to those
59 observed in *piezo1b* morphants (Suppl.Fig.S6.B-D.). These data strongly indicate that genetic
60 compensation has occurred in homozygous *piezo1b*$^{mmr5/mmr5}$ embryos but more importantly,
61 when compensation is inhibited with NMDI, *piezo1b*$^{mmr5/mmr5}$ embryos develop defective aortic
62 valves indicating that *piezo1b* is required for aortic valve development.
63

64 **Zebrafish cardiac performance analysis**

65 The heart is at the centre of the circulatory system and consequently any reduction in its
66 performance will have wide ranging consequences. Using the μZebraLab™ system from
67 ViewPoint [9], we were able to determine that *piezo1b* morphant embryos had a significantly
68 lower heart rate (160.4bpm +/-3.4SEM) than WT embryos (187.5bpm +/- 0.65SEM) (Fig.2.E).
69 To investigate this phenotype further, we next analysed a number of blood flow parameters
70 using the ViewPoint ZebraBlood™ system [9]. In this manner we were able to determine that
71 the mean blood flow in *piezo1b* morphants was significantly lower than that of un-injected
72 controls (Fig.2.F). Further analysis of *piezo1b* morphants indicates that the maximal blood flow
73 (corresponding to cardiac systole) is also markedly reduced when compared to the control
74 embryos (Fig.2.G). Similarly, the average stroke volume is also significantly lower in the

piezo1b morphants when compared to un-injected controls (Fig.2.H). The reduced blood flow rate associated with systole could also be an indicator that cardiac contractility is compromised in *piezo1b* morphants. To test this we made high-speed video recordings of either wildtype un-injected embryos or *piezo1b* morphants. Subsequent frame by frame analysis allowed us to measure the distance that the ventricular wall contracts during a cardiac cycle (Suppl.fig.S5,B). In this manner, we found that ventricular contraction in *piezo1b* morphants was increased resulting in a reduced end systolic volume (ESV) (Fig.2.I). Furthermore, we were also able to observe blood regurgitation occurring between the atrium and ventricle at the end of systole (movies S1 and S2). Taken together, the decreased ESV and cardiac output observed in *piezo1b* morphants suggests the presence of OFT stenosis.

Zebrafish strains and husbandry.

Zebrafish were maintained under standardized conditions and experiments were conducted in accordance with local approval (APAFIS#4054-2016021116464098 v5) and the European Communities council directive 2010/63/EU. Embryos were staged as described [10]. The *Tg(fli1a:GFP)y1Tg* was provided by the CMR[B] *Centro de Medicina Regenerativa de Barcelona.* The double transgenic line *Tg(fli1a:GFP)y1;Tg(cmlc2a:RFP)* was generated in house. All larvae were euthanised by administration of excess anaesthetic (Tricaine).

Morpholinos and injections

Morpholino oligonucleotides (MOs) were obtained from Gene Tools (Philomath, OR, USA) and injected into one-cell stage embryos. The Pz1b MO1 and MO2 target the intron 7/exon 8 and the last exon/intron splice site of *piezo1b* (GenBank: KT428876.1) respectively (supplemental information).

100

101

102 **Embryonic zebrafish endothelial primary cell culture.**

103 3dpf *Tg(fli1a:GFP)y1* embryos were placed in a microtube and pipetted up and down 10 times
104 to remove the yolk sac. Digestion was performed in digestion buffer (2.5mg/mL trypsin, 1mM
105 EDTA, 0.16mg/mL tricaine in PBS) in the incubator (28ºC) and monitored every 10 minutes
106 and pipetted up and down to dissociate cells mechanically. The reaction was stopped by adding
107 a same volume of 10% FBS, 2mM $CaCl_2$. Cells were pelleted by centrifugation 3 min 3000rpm,
108 washed with culture medium (L-15, 5% FBS, 1% penicillin/streptavidin) and re-suspended in
109 culture medium. Cells were plated in a 35mm Petri dish (5 embryos/2mL/per dish) and placed
110 in an atmosphere of 95% air/5% CO_2 at 30 °C for a minimum 2 hours prior to patch clamp
111 experiments.

112

113 **Cell surface quantification**

114 For membrane expression quantification of the WT and variant PIEZO1, fluorescence intensity
115 (grey value) was measured across a line from the outside to the inside of the cell for GFP and
116 RFP using ImageJ.

117

118 **PIEZO1 3D structure**

119 Residues K2528 (Magenta) and Y2038 (Green) identified in this study as subject to genetic
120 variability are represented as spheres. Images were produced using PyMOL ™ Molecular
121 Graphics System, Version 1.8.6.0.

122

123 **CRISPR/Cas9**

124 *Piezo1b* target sequences were identified using ZiFiT online software [11]. The *piezo1b* gRNA
125 was synthesised from a DNA string template from Invitrogen using the Megashortscript T7 kit
126 (Ambion) and purified by phenol/chloroform extraction. 150pg of *piezo1b* gRNA was co-
127 injected with nls-Cas9 protein (N.E.B). Embryos were bred to adulthood and initially screened
128 for mutations in *piezo1b* using a previously described T7 assay [12]. The founder of the
129 *piezo1b*^{mmr5} mutant line was verified by Sanger sequencing and outcrossed to AB wildtype. F1
130 *piezo1b*$^{mmr5/+}$ adults were identified using the T7 assay and verified by Sanger sequencing.
131

132 **PKI166 and AG478 treatments**

133 PKI166 AND AG1478 treatments were performed as described [13].

134

135 **Electrophysiology**

136 Each current was evaluated using an Axiopatch 200B amplifier (Axon Instrument, USA), low-
137 pass filtered at 3kHz and digitized at 2kHz using a 12-bit analog-to-digital digidata converter
138 (1440A series, Axon CNS, Molecular devices, USA). Results are expressed as mean ± standard
139 error of the mean (SEM). Patch clamp pipettes were pulled using vertical puller (PC-10,
140 Narishige) from borosilicate glass capillaries and had a resistance 1.2-2MΩ for the inside out
141 currents. For the whole cell attached currents, the bath solution contained (in mM) 155 KCl, 3
142 $MgCl_2$, 5 EGTA and 10 HEPES adjusted to pH7.2 with KOH. The pipette solution contained
143 (in mM) 150 NaCl, 5 KCl, 2 $CaCl_2$, and 10 HEPES adjusted to pH7.4 with NaOH.
144

145 ***In situ* hybridisation**

146 The *piezo1b* probe was generated by cloning a 2kb fragment from a 3dpf zebrafish cDNA
147 library into pGEMT. The *cmlc2a* probe was generated from pBSK *cmlc2a* containing the full

148 length *cmlc2a* gene. The *elnA and elnB* probes were generated by cloning a 1kb fragment from
149 a 3dpf zebrafish cDNA library into pGEMT.
150
151 **Immunohistochemistry**
152 Transfected cells were fixed in 4% PFA for 20min and blocked with PBS, 2mg/mL BSA, 2%
153 lamb serum for 45min at room temperature. Cells were then incubated in the same solution
154 with primary rabbit anti-Piezo1 antibody (Proteintech 15939-1-AP, 1/100) for 3h followed by
155 donkey Alexa Fluor 594-anti rabbit (Jackson ImmunoResearch Laboratories, 1/200) 2h at room
156 temperature. For whole mount immunohistochemistry, embryos were fixed overnight at 4°C in
157 a solution of 4% paraformaldehyde in PBS. After fixation, samples were washed in PBS with
158 0.1% Tween-20 (PBST), permeabilized with acetone for 6 minutes at -20ºC and blocked at
159 room temperature with 10% bovine serum albumin in PBST. Primary antibody incubation was
160 conducted overnight at 4°C in blocking buffer with the anti-ELNB antibody at a 1:250 dilution
161 . Secondary-antibody incubation was conducted for 3 hours at room temperature in PBST with
162 a Cy3 anti-rabbit (Jackson Labs) at a 1:500 dilution.
163
164
165 **RT-PCR analysis**
166 30hpf embryos non-injected or injected with 5ng of *piezo1b* MO1 or with 5 or 10ng of *piezo1b*
167 MO2 were collected and RNA was isolated with TRIzol® Reagent. RT-PCR was performed
168 on 1µg of RNA using oligo-dT primers and amplification PCR was performed using *piezo1b*
169 specific primers
170 The sequences of the *piezo1b* specific primers are the following:
171 For (MO1): 5'-GTTTTGATCGTAACGTCAAA-3'
172 Rev (MO1): 5'-TCAGTTGTTTGTGTCTCTTT-3'

173 For (MO2): 5'-ACGGAGTCTATAAGAGCATC-3'

174 Rev (MO2): 5'-TCATTTGTTTTTCTCTCGCG-3'

175

176 **Cardiovascular parameters analysis**

177 To determine the cardiovascular parameters, we utilized μZebraLab™ software from
178 ViewPoint which has been developed specifically for this purpose. All experiments were
179 performed as described previously [9]. To determine the mean blood flow, the average of the
180 blood flow values was calculated from a 10 second time frame (1,300 frames). For the
181 maximum and minimum blood flow, averages of highest and lowest peak values were
182 calculated during 20 heartbeats. Stroke volume was calculated by dividing the average blood
183 flow (nL/sec) by the heart beat per second (BPM/60). To assess the heart contractility, movies
184 were recorded at 120fps and measurements were made using ImageJ software.

185

186 **Confocal Imaging**

187 Still images of fixed or anesthetized embryos were recorded using a ProgRes CF colour camera
188 (Jenoptik) mounted on a SZX16 stereomicroscope (Olympus). Fluorescent embryonic heart
189 images were acquired with a Leica TCS SP8 inverted confocal laser scanning microscope with
190 a 20X or 40X oil immersion objectives. Maximal projections and analysis were performed with
191 Imaris or ImageJ softwares. OFT movements were recorded using a high speed 12kHz resonant
192 scanner. Image acquisition and image analysis were performed on workstations of the
193 Montpellier RIO Imaging facility of the Arnaud de Villeneuve/IFR3 campus.

194

195 **PCGC data analysis**

196 Whole exomic data for individual probands was downloaded from the NIH/dbGaP repository
197 (The Pediatric Cardiac Genomics Consortium (PCGC)). The data was subsequently converted

198 into the Fastq format using the SRA toolkit provided by NIH/dbGaP. The exomic data was
199 aligned to the human reference genome and SNPs associated with *PIEZO1* were identified
200 using the Integrative Genomics Viewer [14]. Patients' data analysis was approved by the
201 INSERM Institutional Review Board (IRB00003888 – Opinion number 15-221).

202

203 **Real-time quantitative RT-PCR**

204 RNA samples were obtained from 4 dpf larvae. Total RNA was extracted with Trizol
205 (Invitrogen) and RT-PCR was performed using the Cloned AMV First-Strand cDNA Synthesis
206 Kit (Invitrogen). For real-time quantitative PCR, we used the SYBR Green I Master (Roche).
207 Cycling parameters were as follows : 95ºC x 10 min, 45 cycles of 95ºC x 15 sec and 60ºC x 30
208 sec followed by 95ºCx 10 min. A measure of 10 ng of total RNA was used per reaction.
209 Quantitative PCR was performed on a Roche LightCycler 480. Samples were run in triplicate.
210 The primer3 software (**http://www.bioinformatics.nl/cgi-bin/primer3plus/primer3plus.cgi**)
211 was used to design primers for short amplicon between 100 and 200 bases. Every primers pair
212 has been verified by Absolute quantification/Fit points and by Tm calling using the LightCycler

tuba1-F	5'-CGGCCAAGCAACACTACTAGA-3'
tuba1-R	5'-AGT TCC CAG CAG GCA TTG-3'

213

Piezo1b-F	5'-AGG AGA AAG CAT TCA GCC CC -3'
Piezo1b-R	5'-CCA GCA GGG GAC TGA ACT TT -3'
Piezo1a-F	5'-ATG ACA TAG GGC CCA GTG GA-3’
Piezo1a-R	5'-TGT CAG CCA GCT GTG ATA CG -3'

214

Normalized relative quantification was performed with the ΔΔCt method and expression fold changes were calculated using the following formula : $e^{(-\Delta\Delta Ct)}$, using the tubulin alpha1 housekeeping gene as a reference.

References

[1] Kwan KM, Fujimoto E, Grabher C, Mangum BD, Hardy ME, Campbell DS, et al. The Tol2kit: a multisite gateway-based construction kit for Tol2 transposon transgenesis constructs. Developmental dynamics : an official publication of the American Association of Anatomists. 2007;236:3088-99.

[2] Shmukler BE, Huston NC, Thon JN, Ni CW, Kourkoulis G, Lawson ND, et al. Homozygous knockout of the piezo1 gene in the zebrafish is not associated with anemia. Haematologica. 2015.

[3] Ranade SS, Qiu Z, Woo SH, Hur SS, Murthy SE, Cahalan SM, et al. Piezo1, a mechanically activated ion channel, is required for vascular development in mice. Proc Natl Acad Sci U S A. 2014;111:10347-52.

[4] Lukacs V, Mathur J, Mao R, Bayrak-Toydemir P, Procter M, Cahalan SM, et al. Impaired PIEZO1 function in patients with a novel autosomal recessive congenital lymphatic dysplasia. Nat Commun. 2015;6:8329.

[5] Fotiou E, Martin-Almedina S, Simpson MA, Lin S, Gordon K, Brice G, et al. Novel mutations in PIEZO1 cause an autosomal recessive generalized lymphatic dysplasia with non-immune hydrops fetalis. Nat Commun. 2015;6:8085.

[6] Rossi A, Kontarakis Z, Gerri C, Nolte H, Holper S, Kruger M, et al. Genetic compensation induced by deleterious mutations but not gene knockdowns. Nature. 2015;524:230-3.

[7] Stainier DYR, Raz E, Lawson ND, Ekker SC, Burdine RD, Eisen JS, et al. Guidelines for morpholino use in zebrafish. PLoS genetics. 2017;13:e1007000.

[8] El-Brolosy MA, Kontarakis Z, Rossi A, Kuenne C, Gunther S, Fukuda N, et al. Genetic compensation triggered by mutant mRNA degradation. Nature. 2019;568:193-7.

[9] Parker T, Libourel PA, Hetheridge MJ, Cumming RI, Sutcliffe TP, Goonesinghe AC, et al. A multi-endpoint in vivo larval zebrafish (Danio rerio) model for the assessment of integrated cardiovascular function. J Pharmacol Toxicol Methods. 2014;69:30-8.

[10] Kimmel CB, Ballard WW, Kimmel SR, Ullmann B, Schilling TF. Stages of embryonic development of the zebrafish. Developmental dynamics : an official publication of the American Association of Anatomists. 1995;203:253-310.

[11] Sander JD, Zaback P, Joung JK, Voytas DF, Dobbs D. Zinc Finger Targeter (ZiFiT): an engineered zinc finger/target site design tool. Nucleic acids research. 2007;35:W599-605.

[12] Jao LE, Wente SR, Chen W. Efficient multiplex biallelic zebrafish genome editing using a CRISPR nuclease system. Proc Natl Acad Sci U S A. 2013;110:13904-9.

[13] Goishi K, Lee P, Davidson AJ, Nishi E, Zon LI, Klagsbrun M. Inhibition of zebrafish epidermal growth factor receptor activity results in cardiovascular defects. Mechanisms of development. 2003;120:811-22.

[14] Robinson JT, Thorvaldsdottir H, Winckler W, Guttman M, Lander ES, Getz G, et al. Integrative genomics viewer. Nature biotechnology. 2011;29:24-6.

258 **Supplemental figure legends**

259 **Figure S1. Alignment of Piezo1a and Piezo1b.**

260 Protein alignment comparing Piezo1a and Piezo1b.

261

262 **Figure S2. *Piezo1b* is expressed in endothelial cells.**

263 (**A-C**) ISH using an antisense *piezo1b* probe. (**A,B**) *Piezo1b* expression can be detected in the
264 heart of zebrafish embryos (black arrowhead) at 24hpf (**A**), 48hpf (**B**). (**C**) *Piezo1b* is also
265 expressed in the developing vasculature present on the yolksac (black arrowhead) and in the
266 tail (white arrowhead) of 4dpf zebrafish embryos. Double fluorescent ISH using antisense GFP
267 (**D,G**) and antisense *piezo1b* (**E,H**) probes, merged images (**F**) indicates endothelial GFP and
268 piezo1b co-localise in the endocardium in *Tg(fli1a:GFP)y1* embryos, but not in the
269 myocardium of *Tg(cmlc2a:GFP)* embryos. V and A in the adjacent cartoon indicate the
270 ventricle and atrium respectively. Scale bars: (**A-C**) 100μm, (**F, I**) 10μm.

271

272 **Figure S3. Pz1b experimental controls.**

273 (**A,B**) RT-PCR analysis of Pz1b MO1 splice morphant embryos. The Pz1b MO1 targets the
274 intron 7/exon 8 splice site. Primers designed against exons 7 and 8 (arrows in (**A**)) are able to
275 amplify the correct 330bp fragment (lower band in **B**) from WT embryo cDNA (lane 3). With
276 morphant embryo cDNA, the final intron has not been spliced out (lane 4) indicating *piezo1b*
277 has been disrupted. The first two lanes correspond to the negative control without reverse
278 transcriptase (RT). (**C-F**) Mouse *Piezo1* RNA can rescue the *piezo1b* morphant phenotype.
279 Representative images of the severity of cardiac oedema: (**C**) no oedema, (**D**) moderate oedema,
280 (**E**) severe oedema. (**F**) Graph indicating the percentage of embryos displaying either no
281 oedema (white), moderate (grey) or severe (black) in either *piezo1b* morphant embryos (Pz1b
282 MO) or *piezo1b* morphants co-injected with 20pg of mPz1 RNA (Pz1b MO+Pz1 RNA) n= the

283 cumulative number of embryos from 5 separate experiments. (**G**) Brightfield image of an un-
284 injected 3dpf *Tg(cmlc2a:GFP)* zebrafish embryo, (**G'**) fluorescent image of the same embryo,
285 GFP can be detected in the heart (green). (**H**) Brightfield image of an Pz1b MO2 injected 3dpf
286 *Tg(cmlc2a:GFP)* zebrafish embryo, (**H'**) Fluorescent image of the same embryo, GFP can be
287 detected in the heart (green), note the linear appearance of the chambers (n=38/40). (**I,J**) RT-
288 PCR analysis of Pz1b MO2 morphant embryos. The Pz1b MO2 targets the last intron/exon
289 splice site (**I**). Primers designed against the final two exons (arrows in (**I**)) are able to amplify
290 the correct 440bp fragment (lower band) from wildtype embryo cDNA (lane 1). (**J**) With
291 morphant embryo cDNA, the final intron has not been spliced out (upper 2,183bp band in lanes
292 2 and 3) indicating *piezo1b* has been disrupted. (**K**) Brightfield image of a 3dpf embryo injected
293 with suboptimal (4ng) concentration of Pz1b MO1. (**L**) *In situ* hybridization using an antisense
294 *cmlc2a* probe indicates heart looping is normal (n=20/20). (**M**) Brightfield image of a 3dpf
295 embryo injected with suboptimal (3ng) concentration of Pz1b MO2. (**N**) *In situ* hybridization
296 using an antisense *cmlc2a* probe indicates heart looping is normal (n=20/20). (**O**) Brightfield
297 image of a 3dpf embryo injected with suboptimal concentration of Pz1b MO1 (4ng) and Pz1b
298 MO2 (3ng). (**P**) *In situ* hybridization using an antisense *cmlc2a* probe indicates heart looping
299 is disrupted (n=20/22). **(Q-R**) Mouse *Piezo1* RNA can rescue the *piezo1b* morphant OFT
300 phenotype. Representative images of the OFT in WT larvae (wt), *piezo1b* morphants (Pz1b
301 MO) and *piezo1b* morphants co-injected with mPz1 RNA (Pz1bMO+mRNA). The white line
302 indicates where the width of the OFT was measured. (**R**) Graph indicating the average width of
303 the OFT in WT (n=10), *piezo1b* morphants (n=10) and *piezo1b* morphants co-injected with
304 mPiezo1 mRNA (n=12) (* p<0,05, ** p<0.01, student's t-test). (**S,S'**) GFP fluorescence in
305 wildtype *Tg(fli1a:GFP)y1Tg* larvae. White arrow head indicates GFP expressing endocardium.
306 (**T,T'**) GFP fluorescence in *piezo1b* morphant *Tg(fli1a:GFP)y1Tg* larvae. White arrow head
307 indicates GFP expressing endocardium. (**U**) Confocal maximal projection image of the

308 vasculature in the trunk of a 3dpf un-injected *Tg(fli1a:GFP)y1Tg* transgenic zebrafish embryo.
309 (**V**) Confocal maximal projection image of the vasculature in the trunk of a 3dpf Pz1b MO1
310 injected *Tg(fli1a:GFP)y1Tg* transgenic zebrafish embryo, white arrowheads indicate defects in
311 vasculature (n=14/15).(Scale bars (**G,G',K,L**) 100μm.
312
313 **Figure S4. Homozygous *piezo1b*$^{mmr5/mmr5}$ knockout zebrafish larvae are compensated.**
314 (**A**) Brightfield image of a 3dpf *piezo1b*$^{mmr5/mmr5}$ zebrafish embryo injected with Pz1b MO. (**B**)
315 Brightfield image of a 3dpf *piezo1b*$^{+/+}$ zebrafish embryo injected with Pz1b MO (black arrow
316 head indicates cardiac oedema). (**C**) Graph depicting the number and genotype of embryos
317 which did not present a phenotype. Data has been pooled form 2 separate experiments. (**D**)
318 Quantitative PCR data indicating that there is no significant change in *piezo1a* gene expression
319 in *piezo1b*$^{mmr5/mmr5}$ zebrafish embryos.
320
321 **Figure S5. *Piezo1b* knockdown perturbs systolic contraction.**
322 (**A,B**) Representative images of contraction analysis using ImageJ software. The distance
323 between the two ventricular walls is first measured at the end of diastole (yellow double headed
324 arrow)(**A**), (**B**) the distance is again measured at the end of systole (white double headed arrow,
325 the difference is indicated by the black double headed arrow).
326
327 **Figure S6. NMDI treatment reveals the compensated phenotype in *piezo1b*$^{mmr5/mmr5}$**
328 **knockout zebrafish larvae.**
329 (**A**) Representative images of NMDI treated wildtype (WT)(n=20) or *piezo1b*$^{mmr5/mmr5}$ zebrafish
330 larvae. The 4 images of NMDI treated *piezo1b*$^{mmr5/mmr5}$ zebrafish larvae depict the range of
331 severity of the observed phenotype along with percentage of larvae displaying each degree of
332 severity (n=38). 2 photon images of aortic valves in 7dpf zebrafish larvae labelled with

333 BODIPY. **(A)** Representative image of the aortic valves in a WT larvae, valves are outlined
334 with a dashed white line (n=8). **(B)** A *piezo1b*$^{mmr5/\,mmr5}$ zebrafish larvae (n=8). Graph depicting
335 the length to width ratio for the left and right valve leaflets measured in 7dpf WT larvae and
336 *piezo1b*$^{mmr5/\,mmr5}$ zebrafish larvae. Error bars indicate SD, ANOVA and Dunnet's multiple
337 comparisons test P<0.01(all samples), student's unpaired homoscedastic two tailed t-test
338 **P<0.01. Scale bars-20μm.
339
340 **Figure S7. Analysis of *piezo1b* expression in EGFR inhibitor treated zebrafish larvae and**
341 ***notch1b* KO larvae.**
342 (**A**) *In situ* hybridisation for *piezo1b* in wildtype (WT), wildtype larvae treated with either
343 AG1478 or PKI166 EGFR inhibitors (WT+AG1478 and WT+PKI166) and *notch1b* KO larvae
344 (*notch1b* $^{-/-}$) or their WT siblings (*notch1b* $^{+/+}$). Data under relevant images shows the results of
345 qPCR analysis for *piezo1b* expression performed on larvae from the 3 different conditions.
346
347 **Figure S8. The *fliEP* promoter drives expression in endothelial cells.**
348 Confocal images of *fliEP* driven tdTomato red fluorescent protein in 3dpf zebrafish larvae. (**A**)
349 Confocal image of the entire vasculature system in a *filEP:tdTomato* zebrafish larvae. (**B-E**)
350 Confocal images of the heart of a *filEP:tdTomato/cmlc2a:GFP* zebrafish larvae. (**B**) tdTomato
351 is expressed in the endocardium (red). (**C**) GFP is expressed in the surrounding myocardium.
352 (**D**) Merged image of (**B**)+(**C**). (**E**) Image (**D**) merged with a brightfield image. (**F**,**G**) Confocal
353 images of the dorsal longitudinal anastomotic vessel (DLAV) of a *filEP:tdTomato* zebrafish
354 larvae. (**F**) tdTomato is expressed in the vascular endothelium. (**G**) Image (**F**) merged with a
355 brightfield image.
356
357 **Movie S1**. **The beating heart of a 3dpf wildtype embryo.**

High speed video recording capturing the beating heart of a 3dpf wildtype embryo. 5 heart beats are shown at 120fps then the same 5 heart beats are shown at 40fps. Blood can be seen entering the atrium and passing to the ventricle before ejection.

Movie S2. The beating heart of a 3dpf *piezo1b* morphant.

High speed video recording capturing the beating heart of a *piezo1b* morphant. 5 heart beats are shown at 120fps then the same 5 heart beats are shown at 40fps. Following the contraction of the ventricle blood can be seen regurgitating back into the atrium.

Movie S3. OFT dynamism of a 48hpf *Tg(fli1a:GFP)y1* embryo.

Resonance laser imaging capturing the dynamic movement of the OFT during systole and diastole. Frames were acquired every 50ms.

Movie S4. Dorsal aorta dynamism of a 48hpf *Tg(fli1a:GFP)y1* embryo.

Resonance laser imaging capturing the dynamic movement of the dorsal aorta during systole and diastole. Frames were acquired every 130ms.

Movie S5. Aortic valves in a 7dpf wildtype zebrafish larvae.

2 photon imaging of a BODIPY labelled 7dpf zebrafish larvae reveals the valves dynamically moving during the cardiac cycle.

Movie S6. Aortic valves in a 7dpf *piezo1b* morphant zebrafish larvae.

2 photon imaging of a BODIPY labelled 7dpf Pz1b morphant zebrafish larvae reveals the valves dynamically moving during the cardiac cycle.

382

383 **Movie S7. Aortic valves in a 7dpf *notch1b* mutant zebrafish larvae**

384 2 photon imaging of a BODIPY labelled 7dpf *notch1b* mutant zebrafish larvae reveals the

385 valves dynamically moving during the cardiac cycle.

386

387 **Movie S8. Echocardiogram of the aortic valve from the Y2022H proband.**

388

389 **Movie S9. Echocardiogram of the aortic valve from the K2502R proband.**

390

Piezo1 mutation	CADD-PHRED	Mutation Taster	UMD Predictor	gnomAD allele frequencies
p.Y2022H (c.6064T>C)	Damaging (27.1)	Damaging (0.58)	Pathogenic (99)	$3.336\ 10^{-5}$
p.K2502R (c.7505A>G)	Damaging (25.6)	Damaging (0.80)	Probably pathogenic (69)	$6.498\ 10^{-3}$
p.S217L (c.650C>T)	Damaging (25.6)	Damaging (0.54)	Pathogenic (78)	Not reported

Table.1. Prediction analysis of *PIEZO1* mutations.

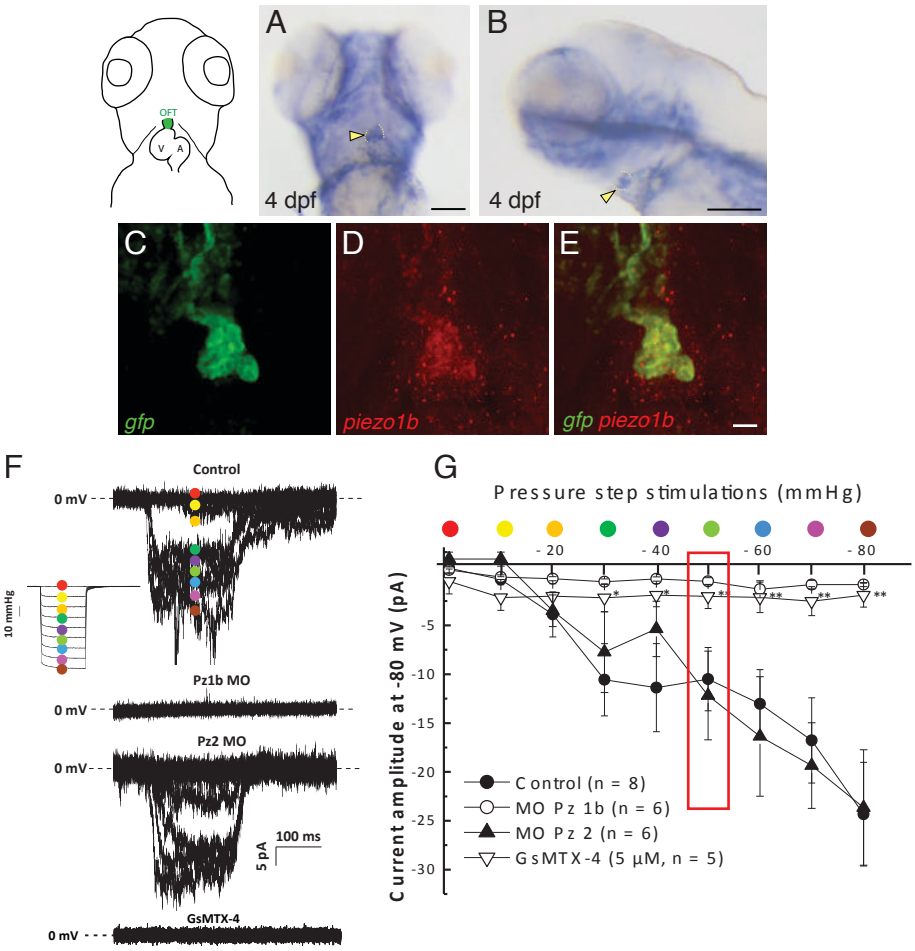
OFT
V
A
A
4 dpf
B
4 dpf
C
gfp
D
piezo1b
E
gfp piezo1b
F
Control
0 mV
10 mmHg
Pz1b MO
0 mV
Pz2 MO
0 mV
100 ms
5 pA
GsMTX-4
0 mV
G
Pressure step stimulations (mmHg)
- 20
- 40
- 60
- 80
Current amplitude at -80 mV (pA)
-5
-10
-15
-20
-25
-30
Control (n = 8)
MO Pz 1b (n = 6)
MO Pz 2 (n = 6)
GsMTX-4 (5 µM, n = 5)

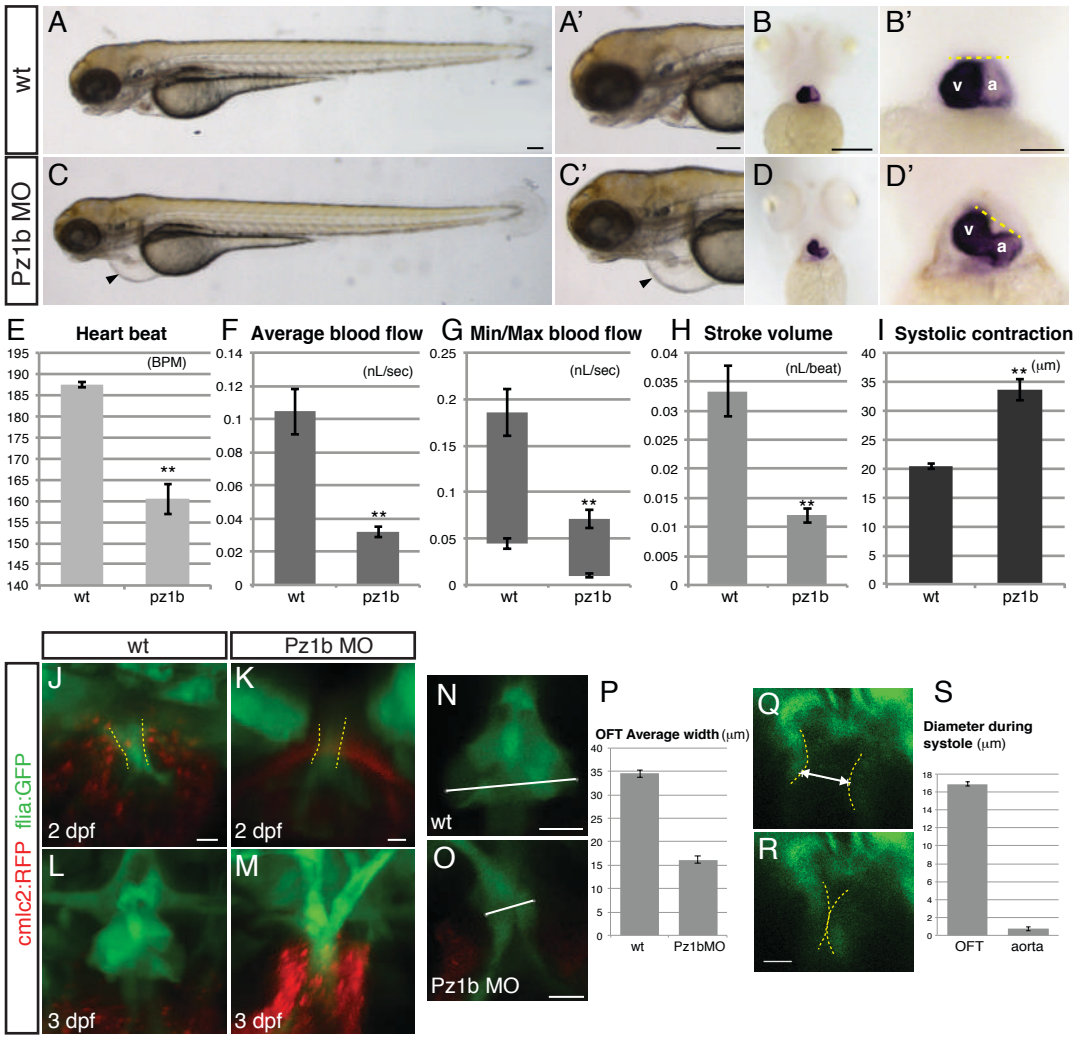
wt
Pz1b MO
A
A'
B
B'
C
C'
D
D'
v
a
E Heart beat
(BPM)
F Average blood flow
(nL/sec)
G Min/Max blood flow
(nL/sec)
H Stroke volume
(nL/beat)
I Systolic contraction
(µm)
wt
pz1b
wt
Pz1b MO
cmlc2:RFP flia:GFP
J
K
L
M
2 dpf
3 dpf
N
O
P
OFT Average width (µm)
wt
Pz1bMO
Q
R
S
Diameter during systole (µm)
OFT
aorta

Faucherre_Figure 3

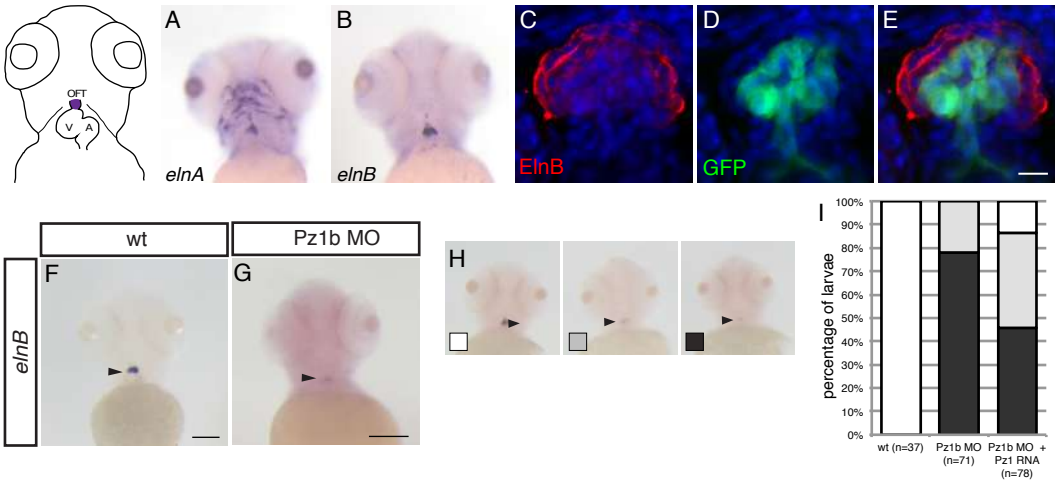

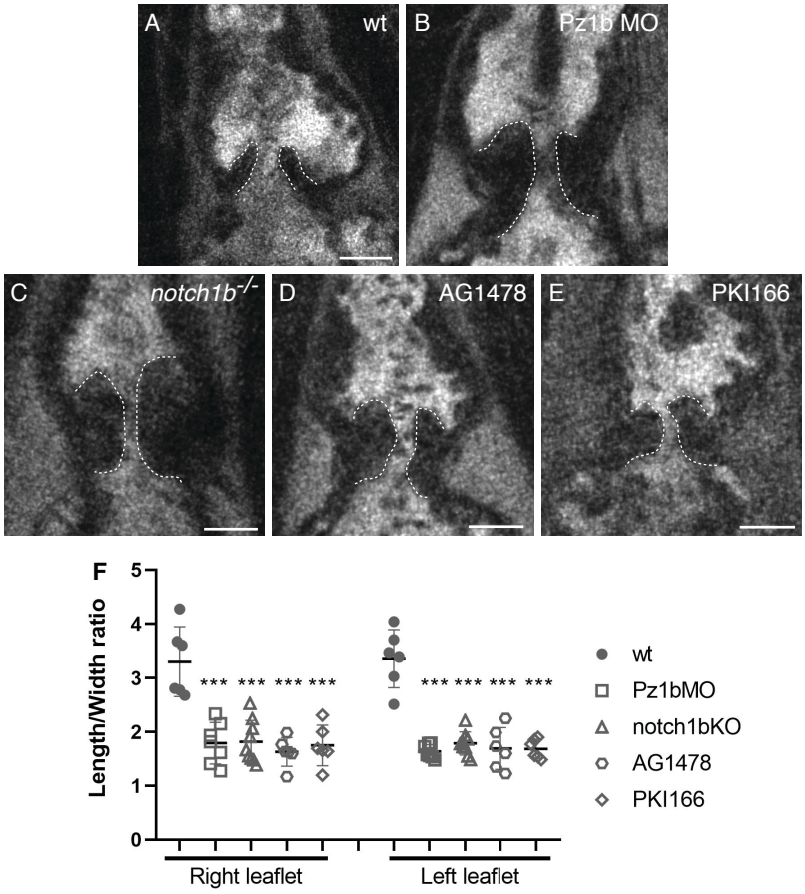
A
wt
B
Pz1b MO
C
notch1b-/-
D
AG1478
E
PKI166
F
Length/Width ratio
0
1
2
3
4
5
***
Right leaflet
Left leaflet
wt
Pz1bMO
notch1bKO
AG1478
PKI166

A

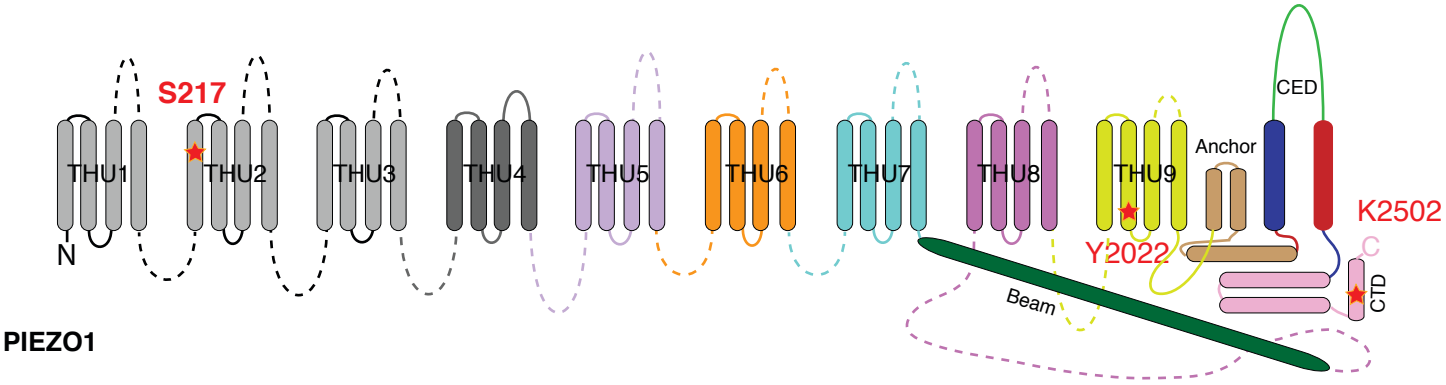

B

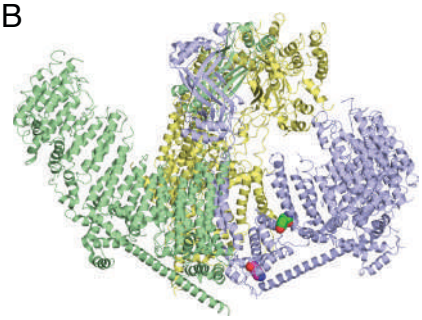

C

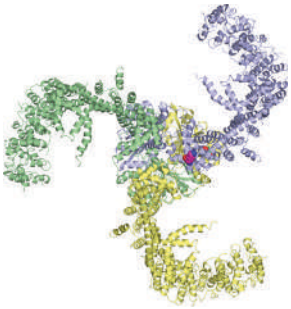

D p.Y2022H

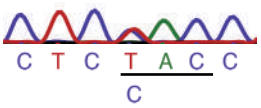

E p.K2502R

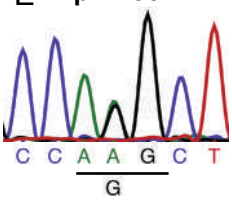

F

	2022	2502	217
human	VDRAL Y LRKTV	EELYA K LIFLY	GIAHP S ALSSV
mouse	IDRAL Y LRKTV	EELYA K LIFLY	GIAHP S AFSSI
chicken	IDRAL Y LRKTV	EELYA K LIFLY	GITLP S ASSSV
zebrafish	VDRAL Y LRKTV	EDLYA K LIFLY	GMMLP S LTSSV
drosophila	IDRAL Y LRKAL	EDLFA K LLFLY	AVLRP S VPGGF
	:**** * ***::	*:*:* * *:***	.: * * ...

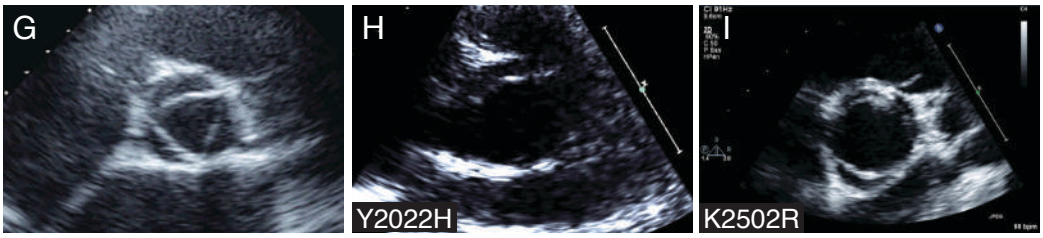

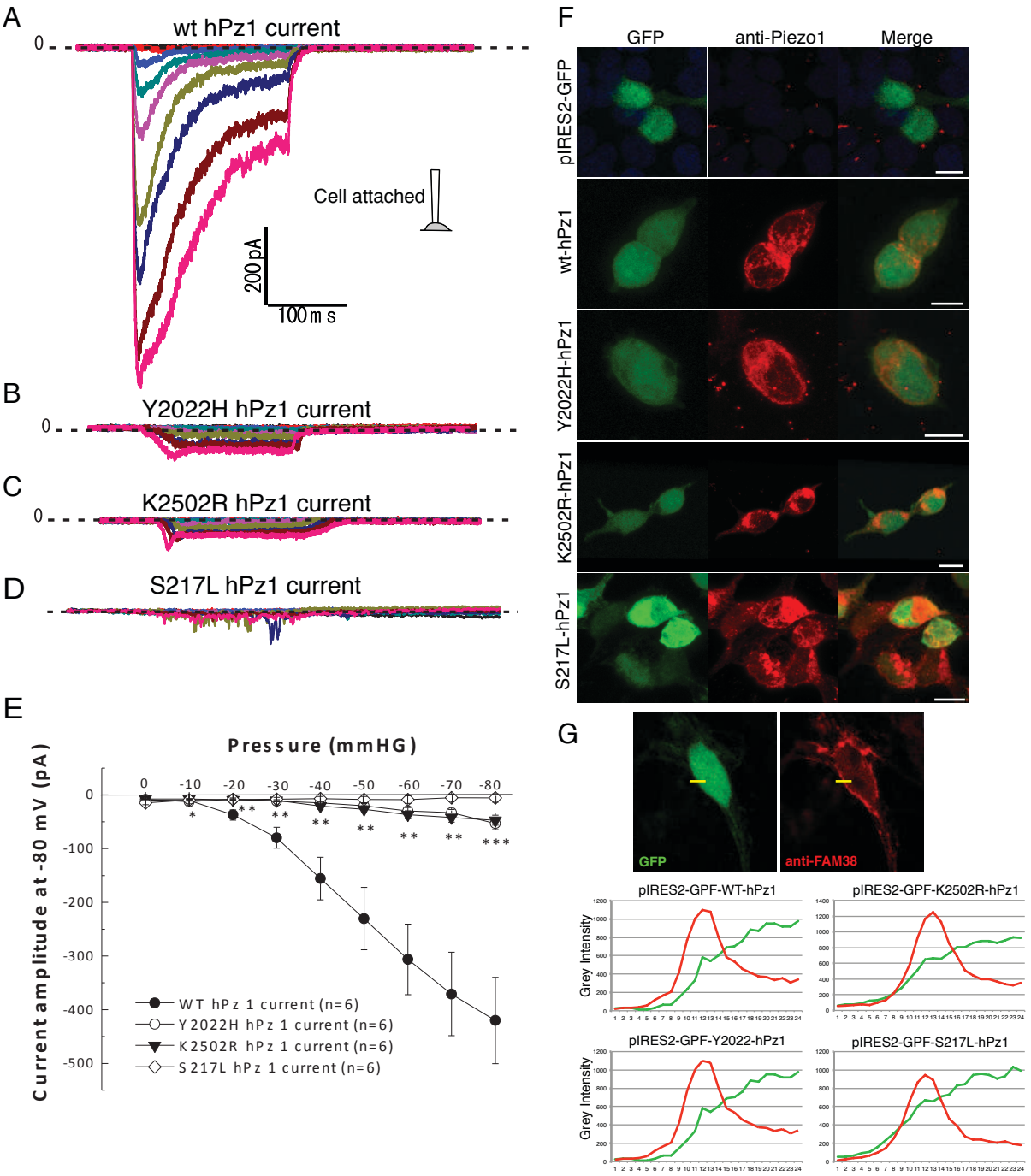
A
wt hPz1 current
0
Cell attached
200 pA
100 m s
B
Y2022H hPz1 current
0
C
K2502R hPz1 current
0
D
S217L hPz1 current
E
Pressure (mmHG)
0
-10
-20
-30
-40
-50
-60
-70
-80
Current amplitude at -80 mV (pA)
0
-100
-200
-300
-400
-500
WT hPz 1 current (n=6)
Y2022H hPz 1 current (n=6)
K2502R hPz 1 current (n=6)
S217L hPz 1 current (n=6)
F
GFP
anti-Piezo1
Merge
pIRES2-GFP
wt-hPz1
Y2022H-hPz1
K2502R-hPz1
S217L-hPz1
G
GFP
anti-FAM38
pIRES2-GPF-WT-hPz1
pIRES2-GPF-K2502R-hPz1
pIRES2-GPF-Y2022-hPz1
pIRES2-GPF-S217L-hPz1
Grey Intensity

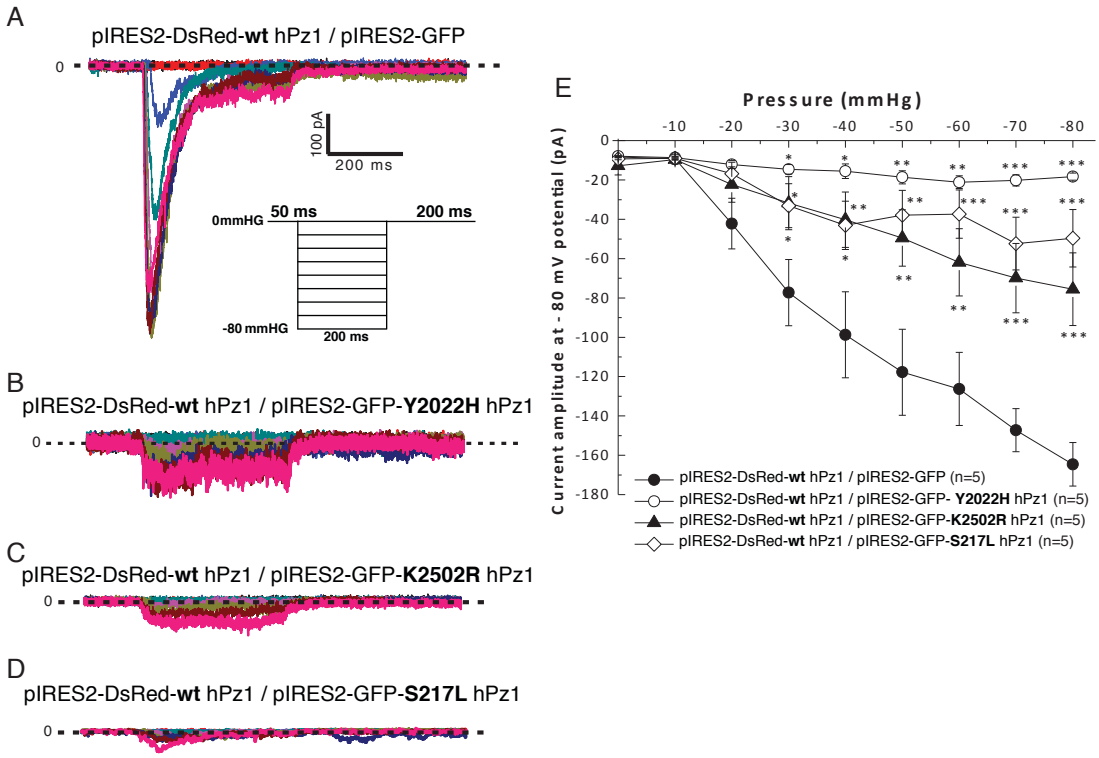
A
pIRES2-DsRed-wt hPz1 / pIRES2-GFP
0
100 pA
200 ms
0mmHG
50 ms
200 ms
-80 mmHG
200 ms
B
pIRES2-DsRed-wt hPz1 / pIRES2-GFP-Y2022H hPz1
0
C
pIRES2-DsRed-wt hPz1 / pIRES2-GFP-K2502R hPz1
0
D
pIRES2-DsRed-wt hPz1 / pIRES2-GFP-S217L hPz1
0
E
Pressure (mmHg)
-10
-20
-30
-40
-50
-60
-70
-80
Current amplitude at - 80 mV potential (pA)
0
-20
-40
-60
-80
-100
-120
-140
-160
-180
pIRES2-DsRed-wt hPz1 / pIRES2-GFP (n=5)
pIRES2-DsRed-wt hPz1 / pIRES2-GFP- Y2022H hPz1 (n=5)
pIRES2-DsRed-wt hPz1 / pIRES2-GFP-K2502R hPz1 (n=5)
pIRES2-DsRed-wt hPz1 / pIRES2-GFP-S217L hPz1 (n=5)

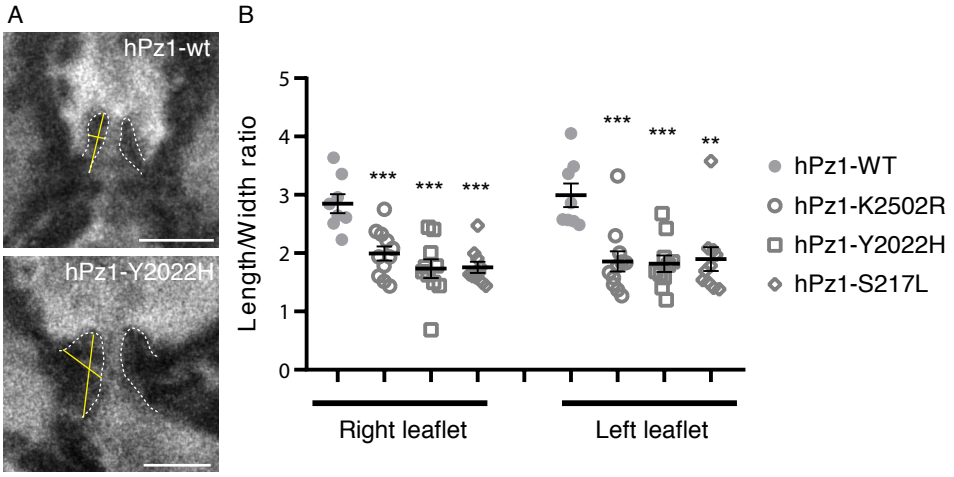
A
hPz1-wt
hPz1-Y2022H
B
Length/Width ratio
5
4
3
2
1
0
***
***
***
***
***
**
Right leaflet
Left leaflet
hPz1-WT
hPz1-K2502R
hPz1-Y2022H
hPz1-S217L

Faucherre_Figure S1

```
CLUSTAL O(1.2.4) multiple sequence alignment


zf_Piezo1a      MELQVVCGLLYCCLLPIFLLAACIFRYNALSLVYLLYLLLLPWFQWPNKHTLRGHTGCYI 60
zf_Piezo1b      MASELLCGLIFRLLLPVCLAAACLFRYNWLSFVYLVFLLLIPLFAEPTHATMTGHTGRLL 60
                *  :::***::  ***: * ***:**** **:***::***:* *  *.: *: ****  :

zf_Piezo1a      KALFSTSLIFILGHVTFQICLYTIPSLDDALGHNCSSWETLSRHVGVSRLPLEDPQGVLW 120
zf_Piezo1b      KVLCLTSVTFLLLHIIFQITVNSLIAGE------------------------------- 88
                *.*  **: *:* *: *** : :: : :

zf_Piezo1a      LLTPDLGVFIMSLITLILCSRLLKKRDEGSVPHMSALLHEADETEDDDEDVEGE-----D 175
zf_Piezo1b      SIQPRFNMFVVSLVTWLLCRSLEKPSIKEDSQHNSDFEVDNQEKEDEEEDENREKRELED 148
                 : * :.:*::**:* :**  * *   : .  * * :  : :*.**::** : *     *

zf_Piezo1a      EGML--------SCSETE--DEE-----------SPS---------SSSAAQLAARLRAT 205
zf_Piezo1b      ELLFEDFELRDGDCELPENEEEEEAADADDGDLEEPDIEESTKTRILRQIADAASKLKEI 208
                * ::        .*.  *  :**           .*.           . *: *::*:

zf_Piezo1a      AQRFLRNMGRILAVTLLALAGITLPSAFSAFYFLLFIGVCTWWACHFPISHLGFNALCVM 265
zf_Piezo1b      VGNLITSAGKVVVTVLLGLTGMMLPSLTSSVYFFTFLGLCTWWSFCRSFDPLLFSCLCVL 268
                . .:: . *:::...**.*:*: ***  *:.**: *:*:****:    :. * *..***:

zf_Piezo1a      VAFFTGGHLVCLYLYQSSFAQAMFSPAGLWARLFGLKDLVTPGNCTTFEVTLNTQYDWPV 325
zf_Piezo1b      MAIFSAGHLVFLYLYQFQFFQEAVPPGNTYASLFGISPVVQTDCSHTWMFKVNPALEWHH 328
                :*:*:.**** ***** .* *  . *.. :* ***:. :*  . . *: ..:*   :*

zf_Piezo1a      YVNPGILLLLYISVTIVLKINSNSLGDADKAREGEAVKTVQGEA-------GEEVELRLW 378
zf_Piezo1b      FVNPIMLLVLYYTLATLIRLWLQESEDTVRDAEAEGKDDAASPENTDINVYTADQRRQLW 388
                :*** :**:** ::: ::::  :.  *: :  *.*. . . .           : . :**

zf_Piezo1a      EARRQSSEDDTK----------QTLL-TTVDSTLS-------------ESHITKEPVIN- 413
zf_Piezo1b      RMAHYHTDERNLLTAQEAYNSPEVLIVTSNGASLDFTSVSHEKRTKCVERNLYSTPHYKA 448
                .  :  ::: .           :.*: *: .::*.             * :: . *  :

zf_Piezo1a      GSSQH-----DIGPS-------------GEATVDNPLRLVGRMVLQQSYICALIAMMVWS 455
zf_Piezo1b      GQPESDTQSLDCGVYRIDSAYVELSELPVAVVRVNSVVKVFRFIMKQSYICALIAMMAWS 508
                *. :      * *                 ..  * :  * *::::***********.**

zf_Piezo1a      ITYHSWLTFVLLLWSCVIWMLRTRQRFAAYCSPFILLYGLALCCLQYVWAMDLETELPQH 515
zf_Piezo1b      ITYVSWLTFVFLIWSCTLWMVRDRRKYSMVTSPFMVFYGNLLIILQYIWSFECLQPVPGL 568
                *** ******:*:***.:**:* *::::   ***:::**  *  ***:*:::    :*

zf_Piezo1a      IGSMSLHQLGLDRAQYPCLRLGALLLFTLTFWLLLRQSVKDTFSRKKS------LTVPLQ 569
zf_Piezo1b      FL----------KKEVPFRELGSKTLCLLSFWLLLRQFLTERREKHTDDPQLSDVTVDGH 618
                :           : : *  .**:  *  *:******* :.:  .::..      :**  :

zf_Piezo1a      EVTTGESTGRNESILKVFGGLVMSLYAKYWIYVCGGMFIMVSFAGKLVAYKIVYMLLFLL 629
zf_Piezo1b      KLGLQDEAAGHREMMEVLGSSLMAMLNKYWIYICGGMFFFVSFEGRIVMYKIIYMMMFLF 678
                ::   :.:. :..:::*:*. :*::  *****:*****::*** *::* ***:**::**:

zf_Piezo1a      CMCLYQVYYSLWRRLLKAFWWMVVAYTMVVLIAIYTFQFEDFPGYWGNFTGFTEQQLADM 689
zf_Piezo1b      CVALYQLHYERWRWMLKYFWMSVVVYTMLVLILVYTFQFESSINVWSNMTGMSREKLEDL 738
                *:.***::*. ** :** **  **.***:*** :******.  . *.*:**::.::* *:

zf_Piezo1a      GLETFKLSELFTSIVIPGFFLLACILQLHYFHKPFMKITDLENVSPIHRKR-----GID- 743
```

```
zf_Piezo1b      GLEKFSVPALFTRIFIPTWFLLVCILHLHYFHERFLELTDIKTVADKQKSTISRLVHLDG 798
                ***.*.:  *** *.** :***.***:*****: *:::**::.*:  ::.       :*

zf_Piezo1a      --------NPDLVQST-EEVRP---------------EEEELIVDQ-------------- 765
zf_Piezo1b      SLVDISMIKPTFNSTNEEEVEKQEDEEDNNYHYENEDEDERVELEEEDVKQTEEQKMEDS 858
                        :* : .:. ***.                *:*.: :::

zf_Piezo1a      -------DDYPSEADEVIPSKWGLVMDRLMVLSRKFSDTLTHVQSFIWRVLELHIVKIVA 818
zf_Piezo1b      LFTCPMTADPVLEQTSELKSKWHLVVERLTVLFLKFLDCIQKLQLFIWWILELHIIKIVS 918
                        *   *  . : *** **::** **  ** * : ::* *** :*****:***:

zf_Piezo1a      FFVVWVALLEPSAMNLVLVVLWSFAMPYGRFRAMASCLSTIWVCVIIVCKMLYQLSVVNP 878
zf_Piezo1b      SYIIWVSVKEVSLFNYVFVVSWAFALPFCQFRPLASSVCTVWTCIIIVCKMLYQLTSISP 978
                 :::**:: * * :* *:** *:**:*: :** :**.:.*:*.*:**********: :.*

zf_Piezo1a      AEYSNNCTAPMVNETSLEPDEVLNSTLYRASVDPASWFGVRKDDTVLGYVKDHLLVLMLL 938
zf_Piezo1b      AAYARNCSMPDNYTE-AQRIDMAKSLLYIGPVDPANWIGLRKFSPLLEYLRNNLLMLALL 1037
                * *:.**: *       :  :: :* ** . ****.*:*:** . :* *:::**:* **

zf_Piezo1a      VFEATVYRHQIHHYRQQQRSPPPIPVIFPQATRDTLDQGLLHCIKYMLNYSFYKFGLEIC 998
zf_Piezo1b      AFEVTIYRHQDFYRMKNNITPPVTRTIFHNITRQHLDDGIVNCAKYFINYFFYKFGLETC 1097
                .**.*:**** .:  ::: :**   .** : **: **:*:::* **::** ******* *

zf_Piezo1a      FLMTVNVIGQRMNFLVIIHGCWLVAIMVRRRRANIATIWSKYCLFLVVFMIYQYVLCVGI 1058
zf_Piezo1b      FLLAVNVIGQRMDFFAMLHAFGLIAVMYQRRRKAIAHVWSKYCCFLACLLSFQYLMCIGI 1157
                **::********:*:.::*.  *:*:* :***  ** :***** **. :: :**::*:**

zf_Piezo1a      PPALCIDYPWRWRSTVTIHSALVKWMYLPDFYTVPNSKNLISDFLLLMCASQQWTVFDNE 1118
zf_Piezo1b      PPAACTDYPWRRS-SSSMDSNVIKWLYFPDFHTKPNSLFLLYDFMLLLCASLQGRVFEEE 1216
                *** * *****   : ::.* ::**:*:***:* ***  *: **:**:*** *  **::*

zf_Piezo1a      KKEEWMVMGGENRDNPDPM---ENMLFNPAPNFINCRSYLDMAKILVFRYMFWFVLSVVF 1175
zf_Piezo1b      CVSPVQLLAGDNVEICRDLDAATFSQHNPVPDFIHCRSYLDMLKVMVFSYLFWFVLTIIF 1276
                  .   ::.*:* :    :       .**.*:**:******* *::** *:*****:::*

zf_Piezo1a      VTGATRISVFGLGYLMACFFFLLFGTKLLTKPSRTRLVMWDCLIIYNVAVIISKNILSIL 1235
zf_Piezo1b      ITGTTRISIFCMGHLVACFYFLIFGGELLLKPIKSILHYWDFLIAYNVFVITMKNILSIA 1336
                :**:****:* :*:*:***:**:** :** ** :: *  ** ** *** **  ******

zf_Piezo1a      ACVFVMEMQKNFCWVIQLFSLVCTVKGYYDPESVCNKDCSLPVEEAGIIWDSICFFFLLL 1295
zf_Piezo1b      ACGYIKALVANHCWLIQLFSLACTIKGYSKPEQQANKQCELPSDEAGIIWDSICFAFLLL 1396
                ** ::  :  *.**:******.**:*** .**. .**:*.** :*********** ****

zf_Piezo1a      QRRVFLSFYFLHVSADLQASARQASRGFELFRASIIKNMHFHQQAERKSIQQLKESMKRI 1355
zf_Piezo1b      QRRVFMSYYFLHVVADIRSSQLLASRGAELFQATIVKAVKARIEEEKKSMDLLKRQMDRI 1456
                *****:*:***** **:::*   **** ***:*:*:* :: : : *:**:: **..*.**

zf_Piezo1a      RGKQQKYKDGRITSDI-------------EEQPSDPKEQKKETKLSKSKSWQYPWVDHAT 1402
zf_Piezo1b      KSRQQKFKRGKERMLSLAQESGERHSVLKEEEEEEEEESSKEKKKGKRKQWWRPWVDHAS 1516
                :.:***:* *:                  **: .: :*..**.* .* *.*  ******:

zf_Piezo1a      VLHSGEYYMFESDSGEEDETFQEEQKPRRQTAFQLAYQAWVTSAKDALKERQQRQRKQRA 1462
zf_Piezo1b      MVRSGNYYLFETDSEEEEEDEDRKDEEPKRSAFQFVYHAWITDSKTAMKERRKEKRRFWQ 1576
                :::**:**:**:** **:*  :.:::  ::::***:.*:**:*.:* *:***::.:*:

zf_Piezo1a      EAEKQQNAQATDDAEEGETVFDGENSQHAEEMQEEGEDAASQATGSDMVQRILDILKFLW 1522
zf_Piezo1b      KYTES-NTNKREQKEANVTVEEGDQDG--------VTEDELSDSPDNMMKRVFNMVKFSW 1627
                :  :. *::  :: * . ** :*::.           :   . : .:*::*::::** *
```

```
zf_Piezo1a      VLFLAMVDGFTMWLNLLTKQYVDTSMVLSEERYLFIHNVSQRASR--ENMD----DQIS- 1575
zf_Piezo1b      VLFLALLDSFTAWLNSICQEHIDISSVLRIERCMLTHEAKKGNVPSRDSIRMYYQRQMCR 1687
                *****::*.** *** : ::::* * **  ** :: *:..:      :.:      *:.

zf_Piezo1a      ----------------------------HDSEDLT----------------LETCLDE- 1589
zf_Piezo1b      PASTQSSLEPTEEAYSDFSPLRTDPDLPPQEHTDLQTSTENLASVYTESSIVEDSTLDEE 1747
                                            ::  **                  :: ***

zf_Piezo1a      -------TDTDNICDTNVVESET-----------LGGFAKSRDFSS--------TTLSS- 1622
zf_Piezo1b      RVLKTSQRSRPKLCRISGVDVSSSADSAASSEHTQGTELYSRQGTSDTVEECGADTLWSS 1807
                        .  ::*  . *: .:            *    **: :*         ** *

zf_Piezo1a      --E--LTLELDCEPFYSQQ------------------------THRPHRSRTASELLSER 1654
zf_Piezo1b      ASDLLQTPHRDVPPSYSRATGLDCICDERKLKIQTPEDSSSGTPQTSSHRLTASELLQTR 1867
                  :   * . *  * **:                          :   :  ******. *

zf_Piezo1a      PFRVDELIQSREFYSSQNRLLKLLFALYNVLAAHSELVCYFIIVLNNLVTASVISLVLPV 1714
zf_Piezo1b      MFYDADLEQSERFYRSQPQLLQLCYSLYNVLVSHSQMVCYLVIILNHMISASVATLVLPV 1927
                 *   :* **..** ** :**:* ::*****.:**::***::*:**:::*** :*****

zf_Piezo1a      LVFLWAMLSVPRPSKRFWMTAIIYTEVMVVVKYLFQFGFFPWNTEYELKLNEDKPFFPPR 1774
zf_Piezo1b      LIFLWAMLSVPRPSKRFWMTAIVYTEVTIVIKYFFQFGFFPFNQSIE--VDKSKPFHPPN 1985
                *:*********************:**** :*:**:*******:* . *  :::.***.**.

zf_Piezo1a      ILGLEKTDNYIRYDLLQLLVLFFHRSLLQRYGLWDQEGPLEEKSDLSPAENSKNENDEKK 1834
zf_Piezo1b      IIGVEKKEGYVHYDLVQLLALFFHRSILKCYGLWDEEEPRSVSPH----THSGAEEKAEC 2041
                *:*:**.:.*::***:***.******:*: *****:* * . . .     :*  *:. :

zf_Piezo1a      FQHSDE-EDSQAQPEPNTEVLSLTPSAETPTDAEIQTDPEPN-SHTNNTKTSDTVKNDGM 1892
zf_Piezo1b      FSEKSPVEDTYTHALSH-THLRLARKQQ--SSAGVRRQSSSISQRSARSKTGSSVSRSSV 2098
                *....  **: ::   :   * *: . :  :.* :: : .   .:: .:**..:*....:

zf_Piezo1a      KKSHFLRFRKKKKAEPDAVQKEPKKKKKKCKTKHSKETSKKLLNAIEGKFKSLFLSVVKN 1952
zf_Piezo1b      R------------------------RSLSAQQKSRKELLMEKLREQLIRAKRFTVKTVLD 2134
                :                        :. ..: *  **   : *.    : * : :..* :

zf_Piezo1a      VYRPTWDFFQNILHAEYRASTDVYALMFLTDVVDFIIIIFGFWAFGKHSAAADIASSLSE 2012
zf_Piezo1b      VYIPIRQFFYSLIHPEYSAVTDVYVLMFLADTVDFIIIVFGFWAFGKHSAAADITSSLSE 2194
                ** *  :** .::* ** * ****.****:*.******:***************:*****

zf_Piezo1a      DQVPEAFLVMLLIQFSTMIIDRALYLRKSILGKLIFQVILVFGIHLWMFFILPAVTERMF 2072
zf_Piezo1b      DQVPEAFLVMVLIQFGTMVVDRALYLRKTVMGKVIFQVILVFGIHFWMFFILPGVTERRF 2254
                **********:****.**::********::::**:***********:*******.**** *

zf_Piezo1a      NHNSVAQLWYFFKCIYFTLSAYQIRCGYPTRILGNFLTKKFNHLNLFLFQGFRLVPFLVE 2132
zf_Piezo1b      SQNTVAQLWYFVKCIYFGLSAYQIRCGYPTRVLGNFLTKSYNYLNLFLFQGFRLVPFLTE 2314
                .:*:*******.***** *************:*******.:*:***************.*

zf_Piezo1a      LRAVMDWVWTDTTLSLSNWMCVEDIYANIFIIKCSRETEKKYPQPKGQKKKRIVKYGMGG 2192
zf_Piezo1b      LRAVMDWVWTDTTLSLSSWICVEDIYAHIFVLKCWRESEKRYPQPRGQKKKKVVKYGMGG 2374
                *****************.*:*******:**::** **:**:****:*****::*******

zf_Piezo1a      LIILFLICIIWFPLLFISLVKSVVGVVNHPVDVTVTVKLGGYEPLFTMSVQQQSIQPFTE 2252
zf_Piezo1b      MIVMLLICIVWFPLLFMSLVKSVAGVVNKPLDVSVTITLGGFQPIFTMSAQQNQLKELTE 2434
                :*:::****:******:******.****:*:**:**:.***::*:****.**:.:: :**

zf_Piezo1a      SRYNQLNNQFSKNAVAMQFITMYSYEDIVTANIEGSSGSVWRISPPSRQELIKELLSSTG 2312
```

```
zf_Piezo1b      SDFKNFINSYNYVPSAMQFLEAYRAEDVTVAELEGSSNSLWTISPPSRKNLMD-VLSKED 2493
                * :::: *.:.    ****:  *  **:..*::****.*:* ******::*:. :**. .

zf_Piezo1a      DMTLRLDWNFQRDLGKGGTVENTFDKHSISLAPKNPVRADLASLLLGTRKDPVHVPHMFP 2372
zf_Piezo1b      QFPVTMTWSIQRNLSLGAKAEFAMDKHVTYLDI--KTRQELIALLNGTRNTPVLIEQVFP 2551
                :: : : *.:**:*. *...* ::***   *     .* :* :** ***: ** : ::**

zf_Piezo1a      NYIRAPSGAEAKPVMQLFDGDEEGFQDVTVSLMREASVNTTGAQEWWDISIAD---CKES 2429
zf_Piezo1b      CFIRAPSDSNAKPIEQLYEDGVY--KSIQLDLER-SANSSEDLQEWWIVDELRSAQKQQR 2608
                 :*****.::***: **::..    :.: :.* * :: .: . **** :.       ::

zf_Piezo1a      CNVLPMIIFNDKVSPPSLGFLAGYGIMGLYVSVVLVIGKFVRGFFSEISHSIMFEELPCA 2489
zf_Piezo1b      EAGLQLYVFSDKVSPPSLGFLAGYGIMGLYASVVLVIGKFVREFFSGISHSIMFEELPCV 2668
                   * : :*.********************.*********** *** ************.

zf_Piezo1a      DRILKLCMDIFLVRETGELELEEELYSKLIFLYRSPETMIKWTREKNHN*     2538
zf_Piezo1b      DRILKLCTDIFLVRETGELELEEDLYAKLIFLYRSPETMIKWTREKNK*-     2716
                ******* ***************:**:********************:
```

Seq1	Length	Seq2	Length	%Identity
zf_Piezo 1a	2538	zf_Piezo 1b	2716	48.22

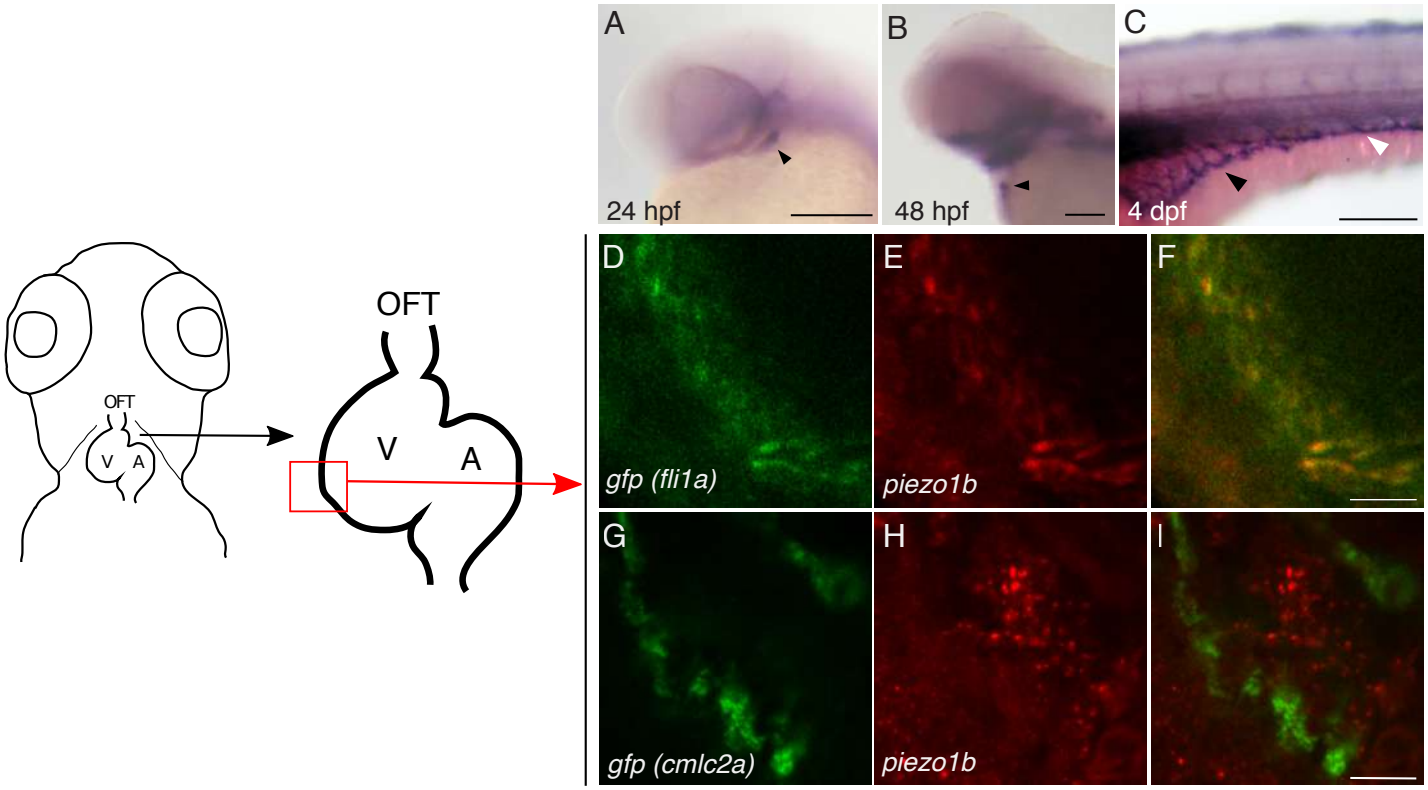
A
24 hpf
B
48 hpf
C
4 dpf
OFT
V
A
OFT
V
A
D
gfp (fli1a)
E
piezo1b
F
G
gfp (cmlc2a)
H
piezo1b
I

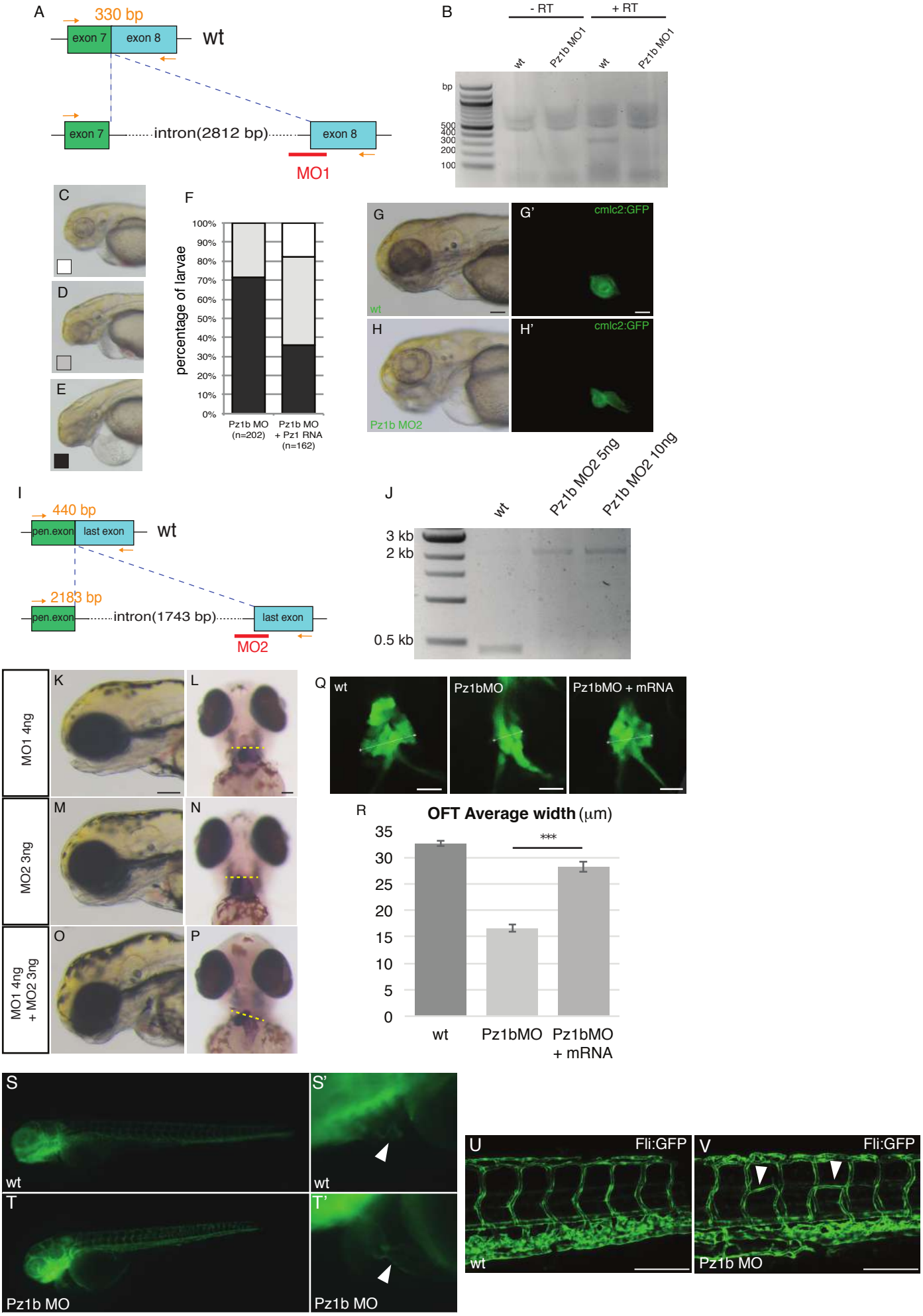
A
330 bp
exon 7
exon 8
wt
exon 7
intron(2812 bp)
exon 8
MO1
B
- RT
+ RT
wt
Pz1b MO1
wt
Pz1b MO1
bp
500
400
300
200
100
C
D
E
F
percentage of larvae
100%
90%
80%
70%
60%
50%
40%
30%
20%
10%
0%
Pz1b MO (n=202)
Pz1b MO + Pz1 RNA (n=162)
G
wt
G'
cmlc2:GFP
H
Pz1b MO2
H'
cmlc2:GFP
I
440 bp
pen.exon
last exon
wt
2183 bp
pen.exon
intron(1743 bp)
last exon
MO2
J
wt
Pz1b MO2 5ng
Pz1b MO2 10ng
3 kb
2 kb
0.5 kb
MO1 4ng
MO2 3ng
MO1 4ng + MO2 3ng
K
L
M
N
O
P
Q
wt
Pz1bMO
Pz1bMO + mRNA
R
OFT Average width (µm)
35
30
25
20
15
10
5
0
***
wt
Pz1bMO
Pz1bMO + mRNA
S
wt
S'
wt
T
Pz1b MO
T'
Pz1b MO
U
Fli:GFP
wt
V
Fli:GFP
Pz1b MO

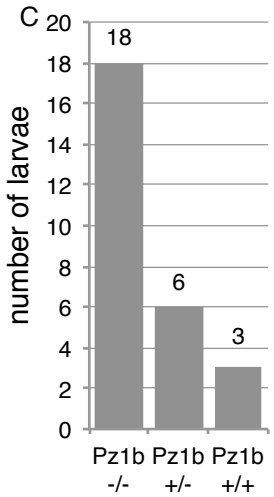

D

Fold change ($e^{(-\Delta\Delta Ct)}$) *piezo1a* expression in *piezo1b*$^{-/-}$ ^{v}/WT	**-0.74** (-0.96; +1.67)

Faucherre_Figure S5

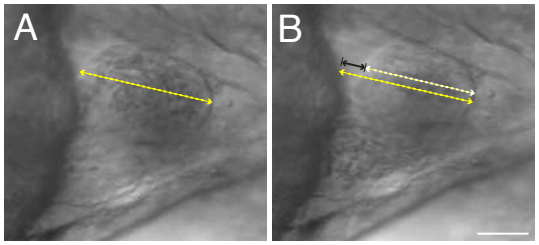

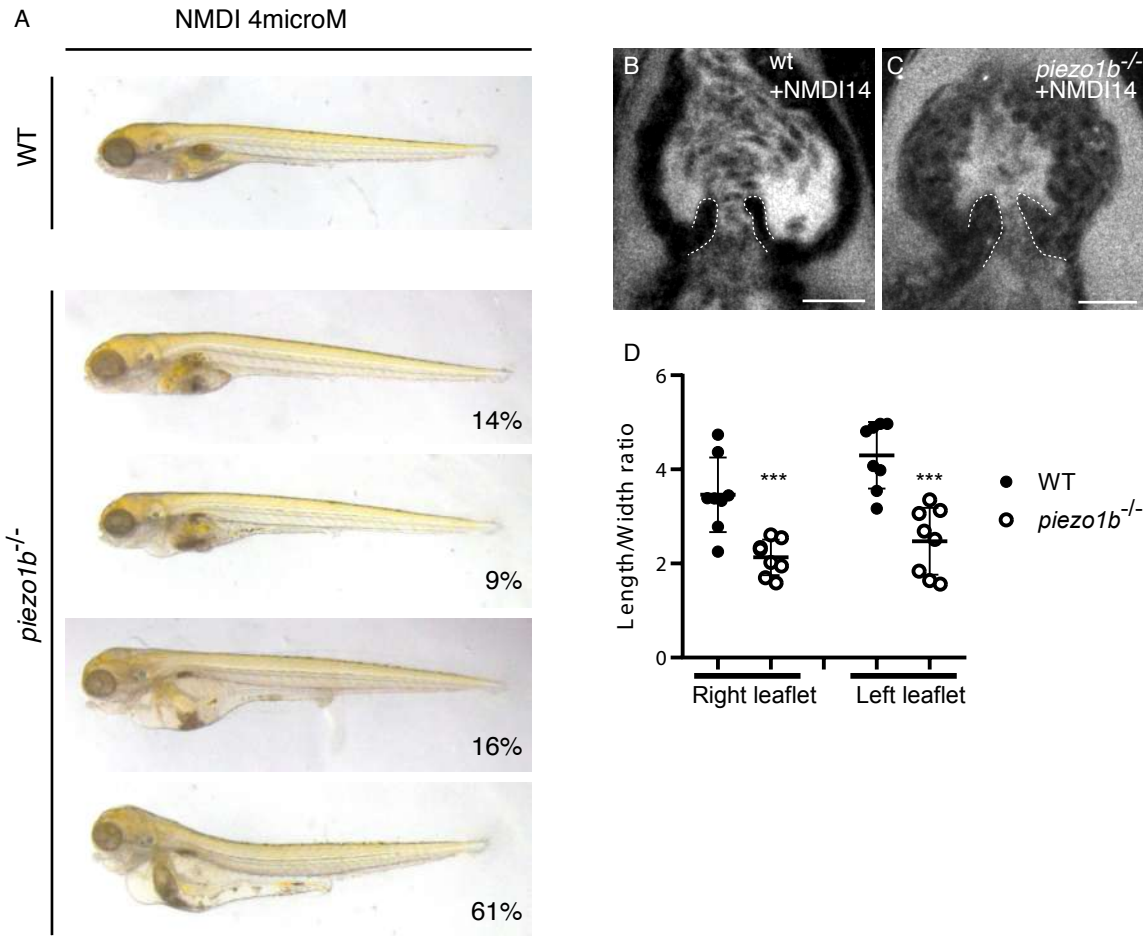
A
NMDI 4microM
WT
piezo1b-/-
14%
9%
16%
61%
B
wt
+NMDI14
C
piezo1b-/-
+NMDI14
D
Length/Width ratio
6
4
2
0
***
***
Right leaflet
Left leaflet
WT
piezo1b-/-

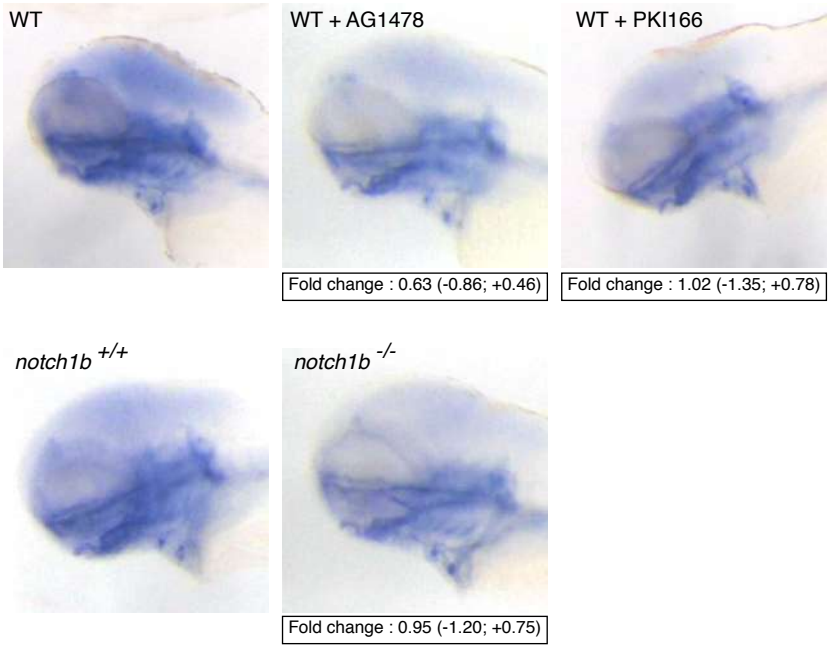
WT
WT + AG1478
WT + PKI166
Fold change : 0.63 (-0.86; +0.46)
Fold change : 1.02 (-1.35; +0.78)
notch1b $^{+/+}$
notch1b $^{-/-}$
Fold change : 0.95 (-1.20; +0.75)

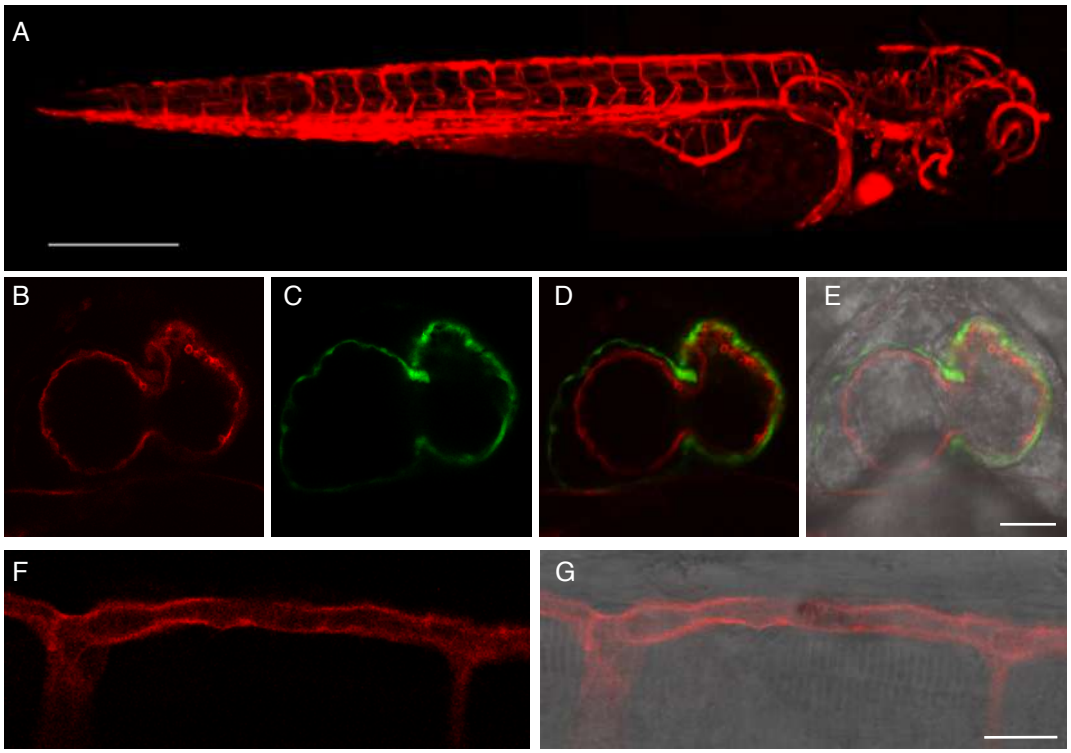
A
B
C
D
E
F
G